hydrology

MDPI

Article

Multi-Model Assessment of Climate Change Impacts on the Streamflow Conditions in the Kasai River Basin, Central Africa

Samane Lesani [1], Salomon Salumu Zahera [1], Elmira Hassanzadeh [1], Musandji Fuamba [1,*] and Ali Sharifinejad [2]

[1] Department of Civil, Geological and Mining Engineering, École Polytechnique de Montréal, Montreal, QC H3C 3A7, Canada; s.lesani@gmail.com (S.L.); salomon.salumu@polymtl.ca (S.S.Z.); elmira.hassanzadeh@polymtl.ca (E.H.)
[2] Aquanty Inc., 600 Weber St. N., Unit B, Waterloo, ON N2V 1K4, Canada; alisharifinejad73@gmail.com
* Correspondence: musandji.fuamba@polymtl.ca

Abstract: The Congo River Basin is the second-largest watershed globally, flowing through nine countries before reaching the Atlantic Ocean. The Kasai River Basin (KARB), containing about one-fourth of Congo's freshwater resources, plays a strategic role in sustaining navigation, food production, and hydroelectricity generation in Central Africa. This study applies a multi-model framework suited for data-scarce regions to assess climate change impacts on water availability in the KARB. Using two conceptual hydrological models calibrated with four reanalysis datasets and fed with bias-corrected outputs from 19 climate models under two representative climate pathways (RCPs), we project changes in the mean annual discharge ranging from −18% to +3%, highlighting the sensitivity of impact assessments to model and input data choices. Additionally, streamflow signatures (Q10, Q50, Q90) are projected to decline by approximately 9%, 18%, and 13%, respectively, under RCP 8.5. Annual hydropower potential is estimated to decrease by 14% and 5% under RCPs 4.5 and 8.5, respectively. These findings provide actionable insights for water management practices in the KARB, including guiding the development of adaptive strategies to optimize water allocation, mitigate risks of scarcity, and support sustainable agricultural and industrial activities in the region.

Keywords: climate change; hydrological modeling; streamflow regime; reanalysis datasets; Kasai River Basin; Congo

Citation: Lesani, S.; Zahera, S.S.; Hassanzadeh, E.; Fuamba, M.; Sharifinejad, A. Multi-Model Assessment of Climate Change Impacts on the Streamflow Conditions in the Kasai River Basin, Central Africa. *Hydrology* **2024**, *11*, 207. https://doi.org/10.3390/hydrology11120207

Academic Editor: Yanfang Sang

Received: 13 November 2024
Revised: 17 November 2024
Accepted: 27 November 2024
Published: 30 November 2024

1. Introduction

Climate change has emerged as one of the most critical challenges of the 21st century, profoundly affecting natural and human systems worldwide. Its impacts on hydrological cycles are particularly significant, altering precipitation patterns, river flows, and water availability. These changes pose severe risks to water resources, agriculture, energy production, and ecosystem health, necessitating comprehensive studies to understand and mitigate potential adverse effects.

Central Africa, home to the Congo River Basin, the second-largest watershed globally, is especially vulnerable to these changes [1,2]. Spanning nine countries and encompassing diverse ecosystems, the Congo River Basin plays a crucial role in regional water security, food production, and energy generation [3]. Within this vast basin, the Kasai River Basin (KARB) is of particular importance, containing about one-fourth of Congo's freshwater resources. The KARB supports navigation, agriculture, and hydroelectricity, making it a strategic area for socio-economic development in Central Africa.

Despite the abundant water budget, high potential for power production, and rich natural resources, the countries herein are the least economically developed and face various food and water security challenges [4,5]. On top of the existing problems, the hydroclimatic conditions of the region have been altered due to the warming climate, which makes sustainable development highly challenging. Alterations in numbers and periods of dry and wet days, a reduction in water content in rainforests, multidecadal drying trends in streamflow, an increase in temperature by 0.5 °C with a stronger increasing trend in minimum than maximum temperatures, and a decline of rainfall by 9% during the 20th century are a few examples of changes in the past few decades [6–11]. The continuation of changes in the climate can cause severe socio-economic vulnerability in the region due to the lack of adequate infrastructure, industrialization, mismanagement, and political issues [10,12–14]. Therefore, understanding the impact of climate change on water availability in the Congo River Basin is essential to propose adaptive water and energy management policies [3].

The impact of climate change can be assessed using the so-called "top-down" approach [15] based on the projections of general circulation models (GCMs), which are downscaled to the spatial resolution of interest and fed into impact assessment models [16]. The GCMs simulate the Earth's physical processes using various mathematical equations, representing mass and energy transfer through the climate system [17]. Due to the inconsistency of GCM projections and the complexity of the Congo River Basin's climate system, using an ensemble of climate models is recommended for impact assessment [3,18,19]. Nevertheless, modeling the impact of climate change on water availability is highly challenging in the Congo River Basin. One of the main problems is the availability of sparse or low-quality hydroclimatic data in the watersheds [20,21]. Even if such data exist, they might be erroneous due to maintenance and operational issues, human errors, and environmental conditions [8,22]. Indeed, the number of active stations in the Congo Basin region has been significantly reduced since the independence of the countries in 1960 [22].

Escalating political issues, a lack of infrastructure such as limited transportation networks, and a limited budget for operation and maintenance are other contributing factors for scarce hydroclimatic stations [21,23,24]. This makes the hydrological representation of catchment physical processes difficult even under the historical conditions in these regions. Hence, some approaches such as regionalization [25] and the use of satellite-derived data [26] or reanalysis datasets [27] have been commonly utilized. Reanalysis is a systematic approach to generate grid-based climate data using data assimilation schemes and models that are fed by available observational data, which are provided from various sources such as satellites, buoys, aircrafts, and ship reports [28,29]. The improved quality and homogeneity of the reanalysis data make them a desirable choice for climate monitoring and research, as well as in commercial applications, particularly in data-scarce regions [27,29]. The hydrological models using reanalysis can estimate river discharge as good as or even better than the ones using the station data [30,31]. Given the differences among reanalysis datasets attributed to inter-model variability, the assimilation approach, and available observations [9,24,32,33], using an ensemble of reanalysis datasets in hydrological modeling is suggested to reduce the related uncertainty.

In addition to limited data, the complexity of catchments, including their size and remoteness, can affect the choice of hydrological models for process representations too [34–36]. The conceptual models have shown acceptable performance and have been suggested to be used in climate change impact studies, specifically in data-scarce regions of the Congo River Basin, due to their simplicity and lower number of variables compared to the other types [33,37–42]. For instance, using GW-PITMAN, it is found that the streamflow characteristics will change in the future, but the magnitude and sign of change are not consistent over the basin [10,19,42,43]. Since the simulation of flow is sensitive to the structure of hydrological models and different models may provide varying flow estimations, it is recommended to use more than one conceptual model for impact assessment [44–48].

The almost unexploited hydropower resource (~68 GW) of the KARB due to financial, political, and infrastructural issues is considered as one of the prioritized components of the sustainable development plan in Africa [49]. However, the high sensitivity of this energy resource to alterations in the streamflow regime makes hydropower production vulnerable to changing climatic conditions. Few studies have analyzed the performance of the water resources system in the KARB in the future [50–53]. While the existing studies on the Congo River Basin use a single hydrological model, e.g., [19,33,42], to the best of our knowledge, a multi-model projection framework has been hindered for impact assessment of the KARB.

Given the strategic significance of the KARB, understanding the impacts of climate change on its water resources is vital. This study aims to assess the impact of climate change on water availability in the Kasai River Basin (KARB; 897,500 km^2), one of the key watersheds in the Congo River Basin, using an ensemble of state-of-the-art reanalysis data, two conceptual hydrological models, and multi-model climate projections under different future scenarios. Containing more than 25% of Congo's freshwater resources with an average annual discharge of 11,500 m^3/s at the reaching point to the Congo River [49], the KARB plays a strategic role in Central Africa's economic growth, with great potential in agriculture, hydropower, mining, and navigation [50].

The paper is structured as follows: Section 2 describes the KARB and its major water resource challenges. Section 3 outlines the framework of the impact assessment, including the datasets and hydrological models used. Section 4 presents the historical performance of the hydrological models and projected flow conditions by the end of the century. The conclusions are highlighted in Section 5.

2. Case Study

The Congo River Basin has an average annual discharge of 40,600 m^3/s and covers an area of about 3.7×10^6 km^2 [54], see Figure 1. It encompasses five sub-watersheds, among which the Kasai River Basin is one of the largest watersheds [7]. Around 72.4% of the KARB is located in Congo, and the remaining part (southwest) is in Angola [55]. The long-term average annual temperature of the basin is about 24 °C [55], and rainfall varies from 1431 to 1515 mm per year [7]. The Kasai River (KAR), with a length of 2153 km, is the mainstream [51], originating from the Munyango headwaters in Angola [43]. The Kwango, Kwilu, and Loange on the left bank of the KAR and Sankuru and Lulua on the right bank are other key rivers in the KARB with an average flow of 2092, 1207, 427, 2500, and 502 m^3/s, respectively [50]. These rivers confluence in Kutu-Moke and have an average annual discharge of 8246 m^3/s at the outlet [22], see Figure 1. The main hydrometric station in the KARB is the Kutu-Moke, covering a drainage area of 750,000 km^2, about 20% of the Congo River Basin [43]. The basin's mean annual rainfall, temperature, streamflow discharge, and drainage area are presented in Table 1.

Table 1. Hydroclimatic characteristics of the KARB.

Climate					Streamflow		
Station	Mean annual precipitation (mm)	Average minimum temperature (°C)	Average maximum temperature (°C)	Basin average precipitation (mm)	Station	Average annual flow (m^3/s)	Drainage area (km^2)
Bandundu	1554	21.4	30.8	1456	Kutu-Moke	8070	750,000
Kiyaka	1649	20.0	29.3				

Containing 360 million cubic meters of the Congo River Basin's water budget per year, the KARB plays a key role in the water resource management of the region [49,56]. Currently, around 25% of the Democratic Republic of Congo's population resides with unequal distribution in the KARB. While most of the population still lives in rural areas, urbanization has been considerable in recent decades [57]. Significant mining resources such as gold, diamonds, and other minerals exist in this region. Nevertheless, shifting agriculture is the primary source of income for most households, which highly depends on water availability in the area. The Kasai River Basin is crucial for sustaining livelihoods, particularly through rain-fed agriculture, which is the primary means of food production in the region. Given the absence of large-scale irrigation systems or significant water storage infrastructure, the natural flow of the Kasai River remains largely undisturbed. This reliance on rainfall highlights the basin's vulnerability to changes in water availability, making it a critical factor for regional food security. A water crisis in this basin could have devastating implications for agricultural productivity and food supplies.

> *Ecologically, the Kasai River Basin is a biodiversity hotspot, hosting rich flora and fauna. It provides habitat for various animal and fish species, some of which are endangered, underscoring the importance of conserving this unique ecosystem. The preservation of these natural habitats is not only vital for biodiversity but also for maintaining the ecological balance and supporting local communities that depend on these resources for their livelihoods.* [58]

> *The basin's unaltered hydrological regime and ecological richness emphasize the need for sustainable water management practices to protect its natural flow and biodiversity against future threats.* [57]

Despite the KARB's potential for power production, agriculture, and rich natural resources, many households have limited access to electricity, safe drinking water, and health services due to the poorly developed infrastructure and political issues [59]. Several rapids and waterfalls flowing into the deep valleys make the KAR and its tributaries strategic for not only navigation purposes but also for hydropower generation, which can promote the region's energy supply. However, the only hydropower plant project in the advanced planning stage is the Katende hydroelectric dam, with a 64 megawatt (MW) planned capacity [57].

As previously noted, changes in climate have already affected Central Africa, including the KARB. The Congo River has faced flow instability during the second half of the 20th century, following a remarkable change by a sharp decline in the last decade [8,55,60,61]. In the KARB, rainfall intensity has dropped by around 9% from 1940 to 1999, with the change in annual rainfall from 1525 mm in 1920–1969 to 1388 mm during 1970–1990 [22]. Such alterations in precipitation have affected the groundwater storage of the basin and have led to reductions in streamflow discharge, e.g., from 8606 m^3/s in 1948–1991 to 6943 m^3/s in 1992–2012 at Kutu-Moke [7].

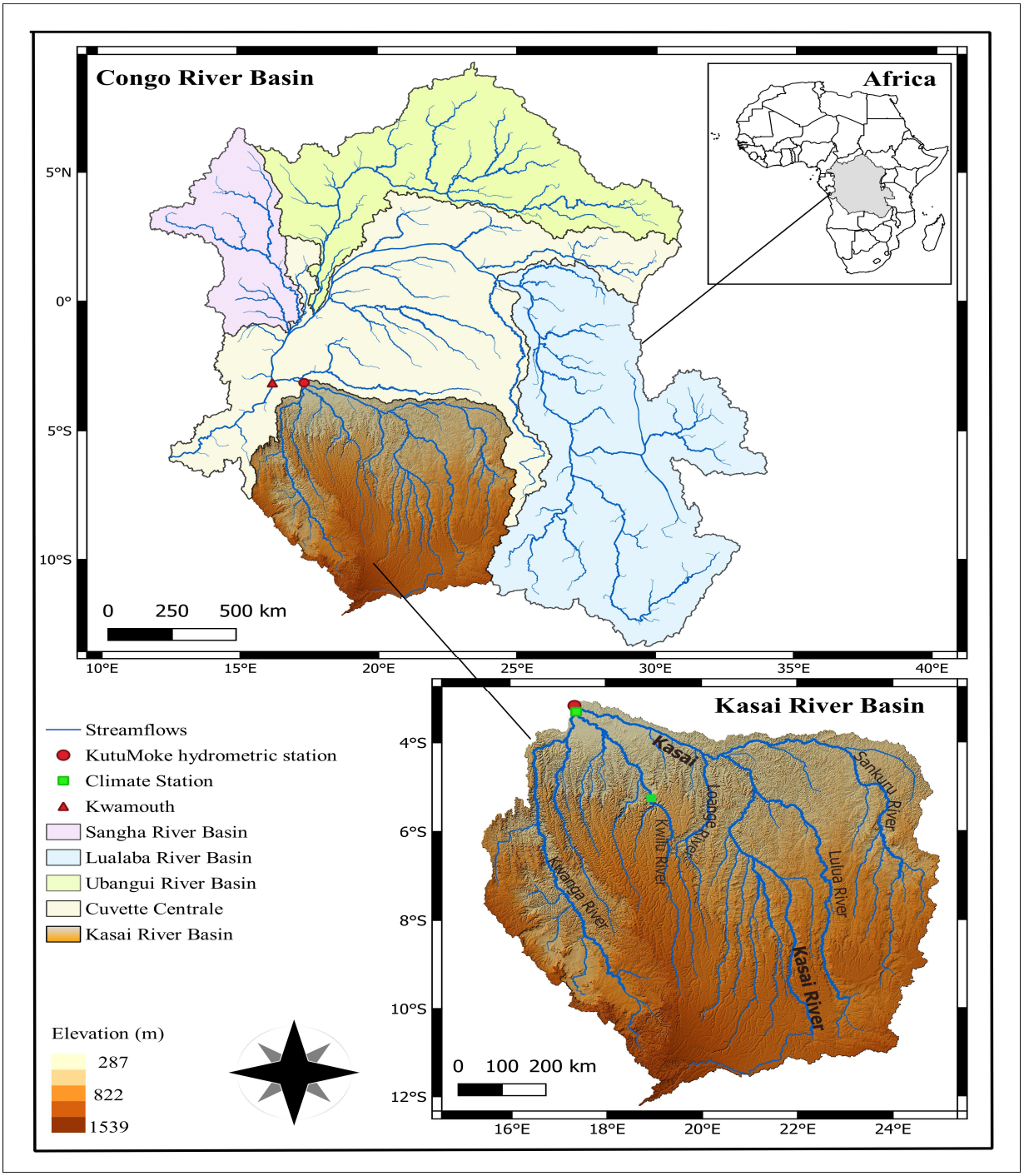

Figure 1. The Kasai River Basin, sub-watershed of the Congo River Basin in Central Africa, and its main tributaries. River networks and sub-basins are retrieved from Linke, Lehner [62].

Using the outputs of GCMs, an increase in between 2 and 6 °C in temperature is projected in Central Africa in the 21st century [3,12,63]. Regarding the precipitation, the projections diverge considerably [12,64,65], and the changes are not homogenous over the basin. For instance, a decrease in precipitation in the south and a slight increase in the north are estimated [19]. As a result, no changes in annual average precipitation over the whole of Central Africa are projected [63]. However, for the KARB, the median of changes in annual total precipitation is projected to increase by around 10% in the late 21st century (2071–2100) under a high-emission scenario. Reductions in precipitation during the dry seasons, i.e., June–July–August and September–October–November, are estimated [63]. The projected

rise in temperature and the decrease or no change in the region's precipitation may lead to prolonged and more frequent dry periods in the future [63]. Moreover, drought-prone areas in the KARB, including savanna parts of the Katanga and the Kasai plateau, are expected to experience seasonal water shortage in the near future [4].

Diverging changes in the streamflow regime in the KARB are estimated based on the rainfall projections and utilized hydrological models [64,65]. For instance, using a global hydrological model with a spatial resolution of 0.5°, more than half of the GCMs in CMIP3 show a decrease in the average annual runoff by 2080 over the basin [66]. In another study, a marginal decrease in average annual runoff in the south and a slight increase (less than 10%) in other regions is projected using a macro-scale VIC hydrological model, forced with bias-corrected outputs of three GCMs in CMIP3 [66]. Such changes in flow make different sectors, including energy, food security, agriculture, the environment, and natural resources vulnerable due to their low adaptive capacity [14]. In these studies, the streamflow is simulated without considering routing through catchments, which may not properly represent flow series at a daily scale. Using a SWAT model for the Congo River Basin and considering an ensemble of GCMs, an increase in the mean seasonal runoff in wet seasons (from December to May) and a reduction in runoff during the dry period in the KARB (from June to November) but an overall increase in annual runoff of the whole Congo River Basin are projected (Aloysius and Saiers) [19]. Nevertheless, there are some limitations in the noted study, such as the calibration of the model using monthly data due to the lack of observed daily streamflow. While in our study, the climate change impacts are assessed utilizing high-resolution GCM projections, the focus is also on understanding the importance of using different hydrological model structures and calibration, which have not been carried out before for this case study to the best of our knowledge.

3. Materials and Methods

3.1. Framework for Climate Change Impact Assessment

Here, we applied a framework suited to the Central African basins to assess the impact of climate change on the KARB, see Figure 2. As previously noted, for these data-scarce regions, most studies suggest using an ensemble of reanalysis data for the calibration of hydrologic models [21,23,28]. Therefore, in this study, a set of state-of-the-art reanalyses along with recorded climate data are used as inputs to hydrologic models. Moreover, HBV and GR4J hydrologic models are used to simulate natural streamflow, with the aim of addressing the inherent uncertainty of the hydrological models and avoiding divergence that may occur using a single model. The calibrated models using these data are forced with the outputs of an ensemble of GCMs under different future scenarios to project water availability by the end of the century. Accordingly, the changes in streamflow characteristics affecting hydropower production are investigated. In the basin under study, there are no existing dams or other water storage reservoirs and thus, these elements are not included in the models. Without such infrastructure, the hydrology of the basin remains largely driven by natural processes, such as precipitation and evaporation, without human-mediated interventions to control or store water. Therefore, the models used in this study focus on the natural hydrological response of the basin to climatic variables, ensuring that the impact assessments and predictions are based on unmodified conditions. This approach provides a clearer understanding of how climate change might affect the basin's natural water resources, without the confounding effects of human-made storage and regulation structures.

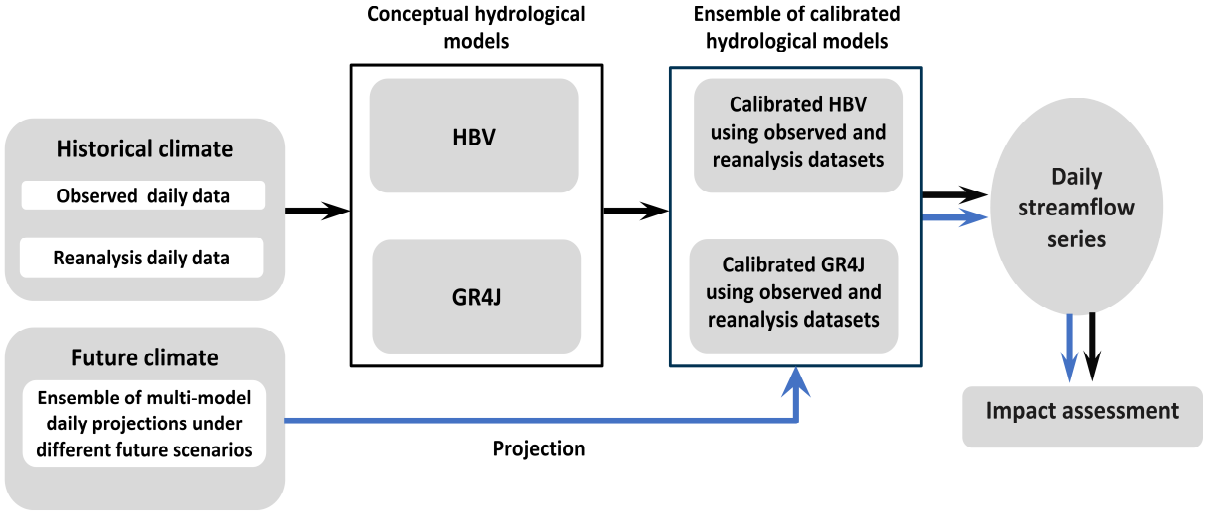

Figure 2. A framework to assess the climate change impacts on water availability in the KARB.

The historical and future climatic data used in this study are described in Sections 3.2 and 3.3, respectively. Section 3.4 describes the employed hydrological models and their calibration and validation procedures.

3.2. Station-Based and Reanalysis Datasets

The streamflow data in the outlet, Kutu-Moke station, is obtained from the International Commission for the Congo–Ubangi–Sangha Basin [22]. Regarding the climate data, the recorded daily precipitation, as well as the minimum and maximum temperature for the KARB, are obtained from the National Meteorological Agency of the Democratic Republic of Congo. Table 1 shows the characteristics of these data. Moreover, the temperature and precipitation data of 4 reanalyses, namely ERA5-land, CFSR, JRA55, and MERRA [23,67], are considered in this study, see Table 2.

Table 2. Utilized reanalysis datasets, their temporal coverage, and spatial and temporal resolutions.

Dataset	Source	Available Temporal Coverage	Spatial Resolution	Temporal Resolution	Reference
ERA5-land	ECMWF	1981–present	0.1° × 0.1°	Daily	Muñoz-Sabater, Dutra [68]
Climate Forecast System Reanalysis (CFSR)	NCEP	1979–present	0.5° × 0.5°	Daily	Saha, Moorthi [69]
Japanese 55-year Reanalysis (JRA-55)	Japan Meteorological Agency	1958–present	1.25° ×1.25°	Daily	Kobayashi, Ota [70]
Modern-Era Retrospective analysis for Research and Applications (MERRA)	NASA GMAO	1979–2016	0.5° × 0.66°	Daily	Rienecker, Suarez [71]

The temporal variation in daily mean precipitation and temperature averaged over the KARB, as well as seasonal cycles of climatic data for each reanalysis product and observed data, are presented in Figure 3. Boxplots and lines contain daily and expected daily temperature and precipitation values over a 30-year period (1981–2010), respectively. Overall, it is evident that the range of reanalysis datasets is different from each other and observed values, particularly considering precipitation. This can be due to divergence

in the assimilation schemes, ground data used in assimilation, and/or utilized forecast climate models, e.g., [32]. Considering the right panel, it is clear that over the Kasai watershed, there are two high-precipitation periods during March–April–May (MAM) and September–October–November (SON). However, the magnitude of rainfall in these wet seasons varies among the reanalysis; MERRA is the most inconsistent dataset, which shows higher differences relative to other datasets. CFSR presents the wettest rainy season, while the JRA-55 data shows the driest season among the reanalysis products. Considering the dry season from June to August (JJA), all reanalyses capture a similar distribution rather than the wet season. Figure 3 shows that all datasets are more consistent in seasonal temperature variation than precipitation, yet the temperature variability in MERRA is more than in others. Overall, the reanalysis provides reliable precipitation and temperature data for the river flow simulation.

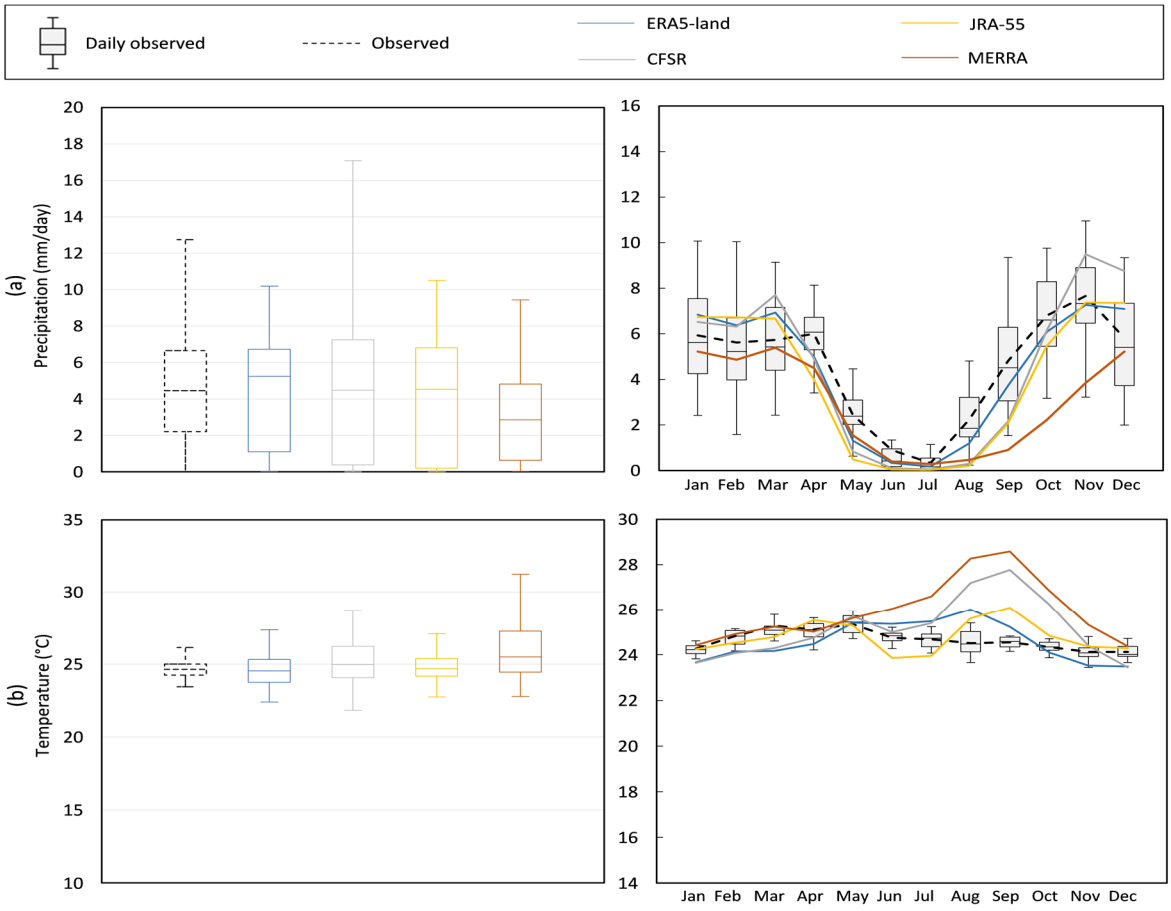

Figure 3. Daily precipitation and temperature values over a 30-year period based on the observed and four reanalysis datasets (**left panel**) averaged over the KARB. The (**right panel**) shows the observed daily (boxplots) as well as expected values (lines) in each month based on observed and reanalysis datasets, which are averaged over the basin.

3.3. Climate Model Projections

In this study, the NASA Earth Exchange Global Daily Downscaled Projections dataset is utilized, which includes data from 19 global climate models (GCMs) across two key representative concentration pathways (RCPs), 4.5 and 8.5, corresponding to the intermediate mitigation and high-emission scenarios, respectively [72,73]. The data include the maximum and minimum air temperature and precipitation with a spatial resolution of 0.25° from 1950 to 2100 for historical and future periods. These pathways are essential for modeling future climate scenarios based on different levels of greenhouse gas emissions.

The use of both RCP 4.5 and RCP 8.5 in this study allows for a comprehensive analysis of potential future climates under different levels of human intervention. By considering both scenarios, the study can compare the impacts of moderate mitigation efforts against a scenario where no significant changes in emissions occur. This dual approach provides a broader understanding of possible future climates and aids in developing robust strategies for climate adaptation and mitigation.

The study examines these scenarios across three time horizons, near-term (2021–2040), mid-term (2041–2070), and long-term (2071–2099), to assess how climate impacts may evolve over time, offering valuable insights for planning and policy development.

Here, 19 GCM simulations during the historical and future periods are compared with each other and reanalysis datasets in Figure 4. Overall, GCMs have a smaller variability than the reanalysis datasets, except MERRA in the historical period, and GCMs have a closer median to ERA5-land. Regarding the temperature, historical GCMs are similar to ERA5-land and JRA-55 in terms of variability, with an almost identical median (around 24.5 °C). In general, our analysis reveals that there is a definite increase in temperature in the future ranging between 1.05 and 2.1 °C and 1.3 and 4.0 °C under RCPs 4.5 and 8.5, respectively. These results are consistent with the findings of previous studies [3,12,63]. Regarding precipitation, a slight increase is expected in the long-term future. The median of projections during the future horizons ranges between 4.33 and 4.42 mm/day and 4.33 and 4.53 mm/day under low- and high-emission scenarios, respectively. These quantiles present around a 1% to 6% increase in the median of daily precipitation with respect to the historical values.

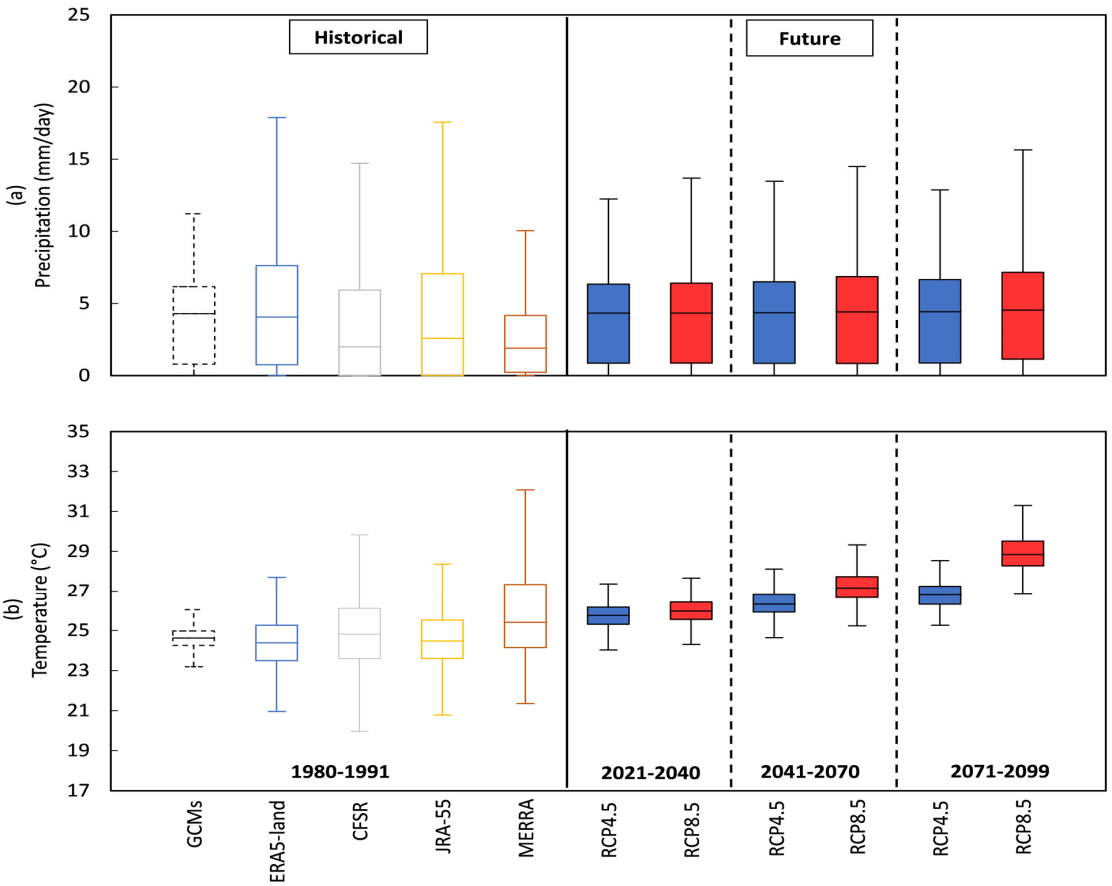

Figure 4. A comparison of (**a**) precipitation and (**b**) temperature in the future based on 19 climate models under RCPs 4.5 and 8.5 (**right**) with respect to the historical values of GCMs and reanalyses (**left**) in the KARB.

3.4. Hydrological Models

As noted earlier, HBV-MTL and GR4J models were used to simulate daily streamflow in the KARB due to their simplicity and accuracy [74]. HBV is widely used [75,76] in climate change impact studies [33,38]. In particular, the model has shown considerable potential for streamflow estimation in ungauged basins [77,78]. HBV-MTL, a recently modified HBV model in [44], is used here. The main inputs to this model are daily precipitation, as well as the maximum and minimum air temperature. The model consists of four main modules, namely soil moisture, surface runoff, interflow, and baseflow reservoirs. The precipitation, either rainfall or snowmelt, enters the soil moisture module. This module evaluates effective rainfall contributing to surface runoff, or the water infiltrates the soil used by vegetation through evapotranspiration. Evapotranspiration is estimated using the Hargreaves method (Hargreaves & Samani, 1985) because of its simplicity and minimum data requirements compared to other methods, especially in such a data-scarce region [79]. The remaining water in the soil is stored in two conceptual reservoirs, the so-called intermediate and deep soil layer, which gradually releases and forms the intermediate and base flow. Finally, the flow at the watershed outlet is stimulated by the accumulation of direct runoff, intermediate flow, and base flow routed through a triangle delay function. For more information about the model structure and equations, see Sharifinejad and Hassanzadeh's study [44].

The GR4J is a lumped model which estimates runoff based on daily temperature, precipitation, and potential evapotranspiration data. Unlike HBV, in GR4J, the net precipitation obtained by subtracting potential evapotranspiration from precipitation is divided into two portions. The model consists of three modules, namely production storage, routing storage, and two unit hydrograph functions. First, a portion of net precipitation is stored in the production storage, from which the water percolates gradually, dependent on the soil moisture capacity. Meanwhile, some of the stored water used by vegetation leads to evapotranspiration. The other portion of the net precipitation integrates with the percolated water from production storage and contributes to the routing storage through unit hydrographs. Indeed, the unit hydrographs in the model address the lag time between precipitation and streamflow generation. In this stage, 10% of the existing water (runoff) is directly routed to the outlet using a two-sided unit hydrograph, while the remaining 90% is routed indirectly through groundwater exchange using a one-sided unit hydrograph. More details about the model structure and equations can be found in Perrin and Michel's study [80].

The model parameterization includes a few steps. In brief, the data during the historical period are divided into three parts for model warm-up, calibration, and validation. The first year of data is used for warm-up to allow for model states to tune out based on the initial conditions of the watershed [76,81]. Then, 66% and 34% of the remaining data are used for model calibration and validation, respectively, based on the split-sample test [44,82]. The two hydrological models are calibrated against observed streamflow using an ensemble of climate datasets during the historical period, including station-based data and four reanalyses, namely ERA5-land, CFSR, JRA55, and MERRA. Accordingly, the models' performance is evaluated based on the Kling–Gupta efficiency (KGE) measure [83], and the value of parameters are obtained for each model. The KGE presents a more comprehensive comparison between the estimated and observed values using different statistical criteria, namely the standard deviation, mean, and Pearson's correlation coefficient, which are shown as α, β, and r in the equations below (Equations (1)–(3)). As shown in Equation (4), these criteria are combined in the KGE in a more balanced way using the Euclidean distance measure compared to other measures such as the Nash–Sutcliffe eficiency [84]. The calibration and evaluation of the models are performed considering this measure at daily and annual scales (Equation (5)). In Equations (1)–(3), σ_s and σ_o are the standard deviations of the simulated and observed flow, $\overline{S}$ and $\overline{O}$ are the mean simulated and observed flow, and S_t and O_t are the simulated and observed flow, respectively.

$$\alpha = \frac{\sigma_s}{\sigma_o} \tag{1}$$

$$\beta = \frac{\overline{S}}{\overline{O}} \tag{2}$$

$$r = \frac{\sum_t (O_t - \overline{O})(S_t - \overline{S})}{\sqrt{(\sum_t (O_t - \overline{O})^2)(\sum_t (S_t - \overline{S})^2)}} \tag{3}$$

$$KGE = 1 - \sqrt{(1-\alpha)^2 + (1-\beta)^2 + (1-r)^2} \tag{4}$$

$$Obj = Min\sqrt{\left(1 - KGE_{daily}\right)^2 + (1 - KGE_{annual})^2} \tag{5}$$

The Shuffled Complex Evolution algorithm (SCE-UA) is used to calibrate the hydrological models [85,86]. In this method, the optimized parameter set is found based on a combination of random [87] and deterministic approaches [88], clustering [89], and competitive evolution [90]. The optimized parameter sets are found in a natural evolution process through a global search. A population (parameter sets) is randomly sampled from the feasible space and then partitioned into several complexes that will evolve independently through the complex competitive evolution technique. To avoid reaching local optima, the entire population is shuffled and the information of complexes is shared. These processes are repeated, since the convergence criteria are satisfied. In this study, 50 populations were selected randomly from the feasible space based on the parameter sets' range and were divided into five complexes. The evolution and shuffling of the independent complexes were repeated until the maximum iteration of 100. As a result, the best parameter sets with the smallest value for the considered objective function (Equation (5)) were obtained. This ensemble of parameter sets is called the "optimal parameter set", leading into an "optimal flow simulation". Besides the use of global optimization in the calibration of the models, to avoid the probable underestimation of the parametric uncertainty [91,92], the generalized likelihood uncertainty estimation (GLUE) was used [93–95]. GLUE is a statistical method employed in hydrological modeling for quantification of uncertainty attributed to the model parameters. Hence, instead of having one optimal parameter set, there will be a range of acceptable parameter sets based on the considered objective function. For this purpose, the initial parameter sets are selected randomly from the feasible range of parameters using a uniform probability distribution. The KGE is used as the statistical criterion to quantify the closeness of the simulated and observed flow and find the acceptable parameter sets. Considering both daily and annual scales, the value of the KGE should be larger than 0.5 to select the "acceptable parameter sets". A total of 10,000 iterations was considered to generate the parameter sets. Using these "acceptable parameter sets", an ensemble of "acceptable streamflow" for each model was estimated.

4. Results

4.1. Performance of the Hydrological Models During the Historical Period

Based on the availability of daily streamflow and climate datasets, 1980–1991 is considered as the historical period for the streamflow simulation. The HBV and GR4J models are calibrated using the observed and four reanalysis datasets. The performance of these models in reproducing the observed streamflow is assessed using the KGE measure, see Table S1 in the Supplementary Materials. The low KGE values, i.e., less than 0.4 and 0.2 for HBV and GR4J models, are not acceptable, which can be attributed to the low quality of the observed station-based data, demystified in various studies [19,34]. Hence, these models are not considered for impact assessment. However, the calibrated models using the reanalysis datasets provide reasonable results. Figure 5 shows the daily and annual time series of the observed and simulated flow using HBV (left) and GR4J (right) models fed with the four reanalysis datasets during the calibration and validation periods, respectively. Considering the simulations, both the optimal set and an ensemble of acceptable flow series corresponding to their parameter conditions, noted in Section 3.4, are presented. Both seasonality in discharge and the overall distribution of discharge (monthly hydrograph) are

simulated well. Moreover, the KGE values above 0.5 for all eight configurations indicate that these models perform better than the calibrated models using the observed data, which is concluded by other researchers as well [30,31].

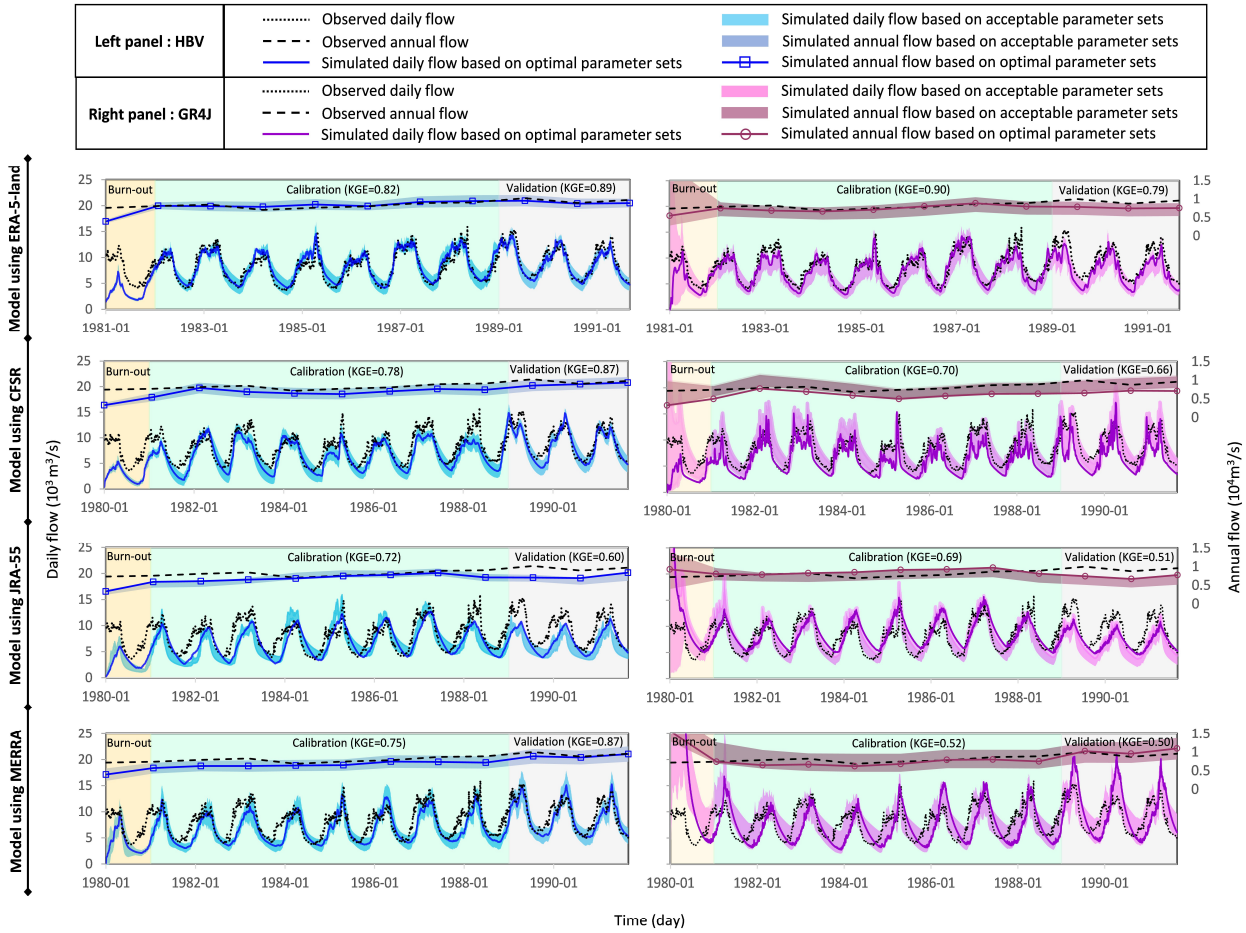

Figure 5. Observed and simulated daily and annual flow during the historical period at the outlet using four reanalysis datasets forced to HBV (**left**) and GR4J (**right**) models.

However, the performance of the models varies depending on the applied reanalysis datasets for calibration, as well as the considered hydrological model [96,97]. Considering both daily and annual time series, it seems that the calibrated models with ERA5-land datasets perform better, in particular, in representing the peak flow timing and magnitude and low flows. Conversely, the models calibrated with MERRA show a larger discrepancy in estimating flow discharge. The impact of input data on flow simulation is more evident at the annual scale. For instance, both HBV and GR4J models using the CFSR dataset continuously underestimate the annual flow during the historical period, while the calibrated models using JRA-55 estimate streamflow more accurately than with the CFSR dataset. It is noteworthy to mention that the ERA5-based models more precisely simulate annual flow by around half of the relative error than other datasets. Besides the input data, it is clear that the structure of the hydrological models is critical in simulating streamflow. For instance, using the MERRA dataset, the HBV model during the validation period (1989–1991) underestimates annual flow, while the GR4J model overestimates it. In addition, the GR4J model better reproduces the daily flow with a lower relative bias (0.05) than HBV (0.1) and a higher correlation coefficient by 0.05 difference, given the ERA5-land dataset. Considering the long-term annual hydrograph of the simulated and observed flow (Figure 6), in the wet season (March–April–May), the HBV model calibrated with ERA5 simulates high flows more accurately than other models (with 2% bias respecting the

observed ones), while GR4J with the same dataset (ERA5-land) shows a larger difference in the simulated peak flow with observations demonstrating around a 7% bias. Meanwhile, the largest bias in estimated flow in the wet season is related to the GR4J model calibrated using the CFSR.

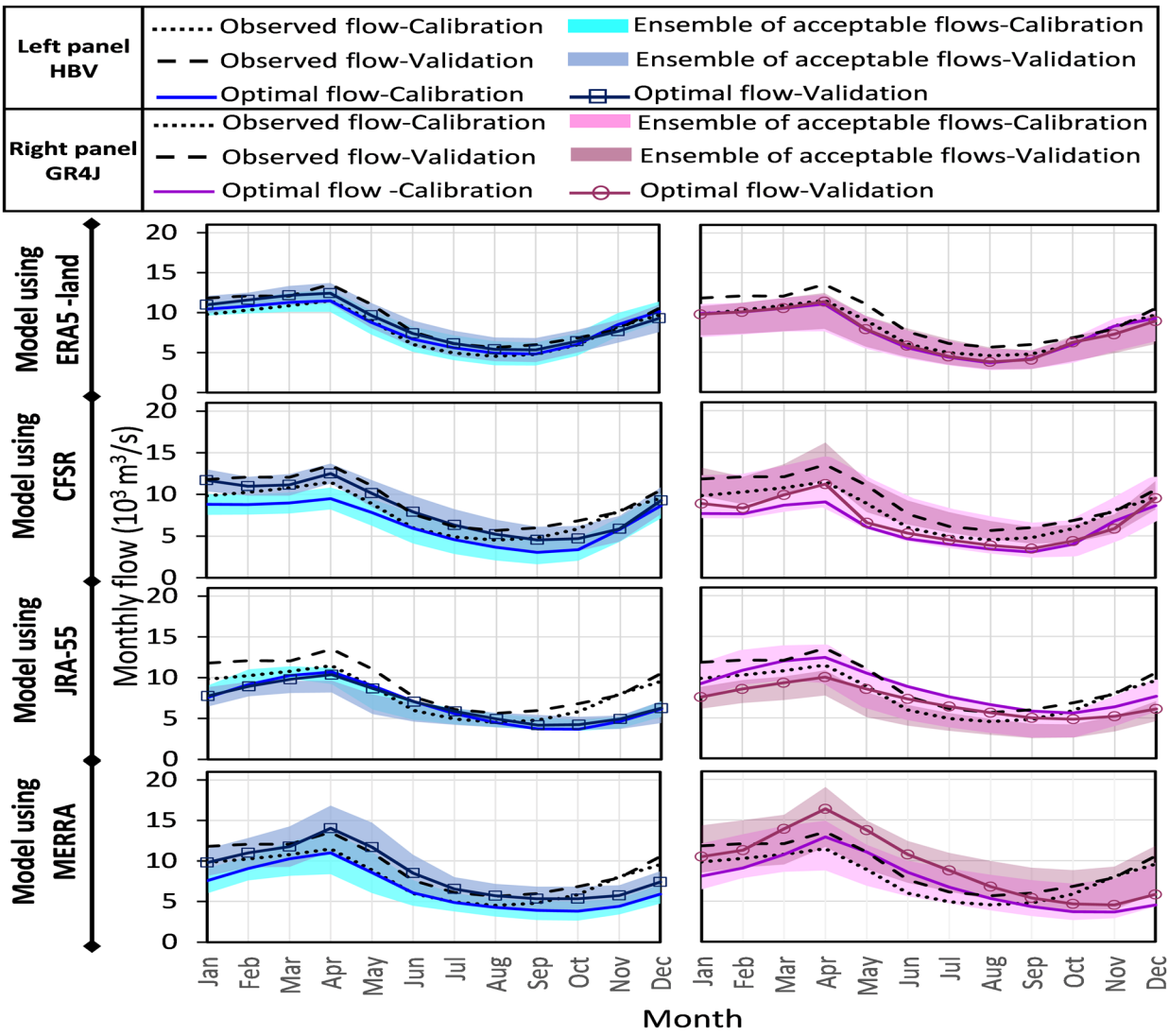

Figure 6. Observed (dashed line) and simulated long-term annual hydrographs (solid line and shaded areas) during the historical period at the outlet using different reanalysis datasets forced to HBV (**left**) and GR4J (**right**) models.

To better understand the differences between the models, the envelopes of simulated flow considering all reanalyses using HBV and GR4J are shown in Figure 7 in the top and bottom rows, respectively. Considering the ensemble of acceptable flow, the GR4J model presents a wider range of values and overestimates daily flows more than the HBV model. During the wet season, GR4J estimates higher values for annual peak flow, e.g., greater than 15,000 m^3/s, while the low flows are approximately the same for both models. It is evident that the shape of the annual hydrograph obtained from the HBV model is more consistent with the observed one, in particular, in the first quarter of the year. However, the difference between the two models, HBV and GR4J, is negligible (less than 5% difference considering the mean annual hydrographs). Since the differences among the performance of these eight configurations are not significant, all of them are used for the impact assessment.

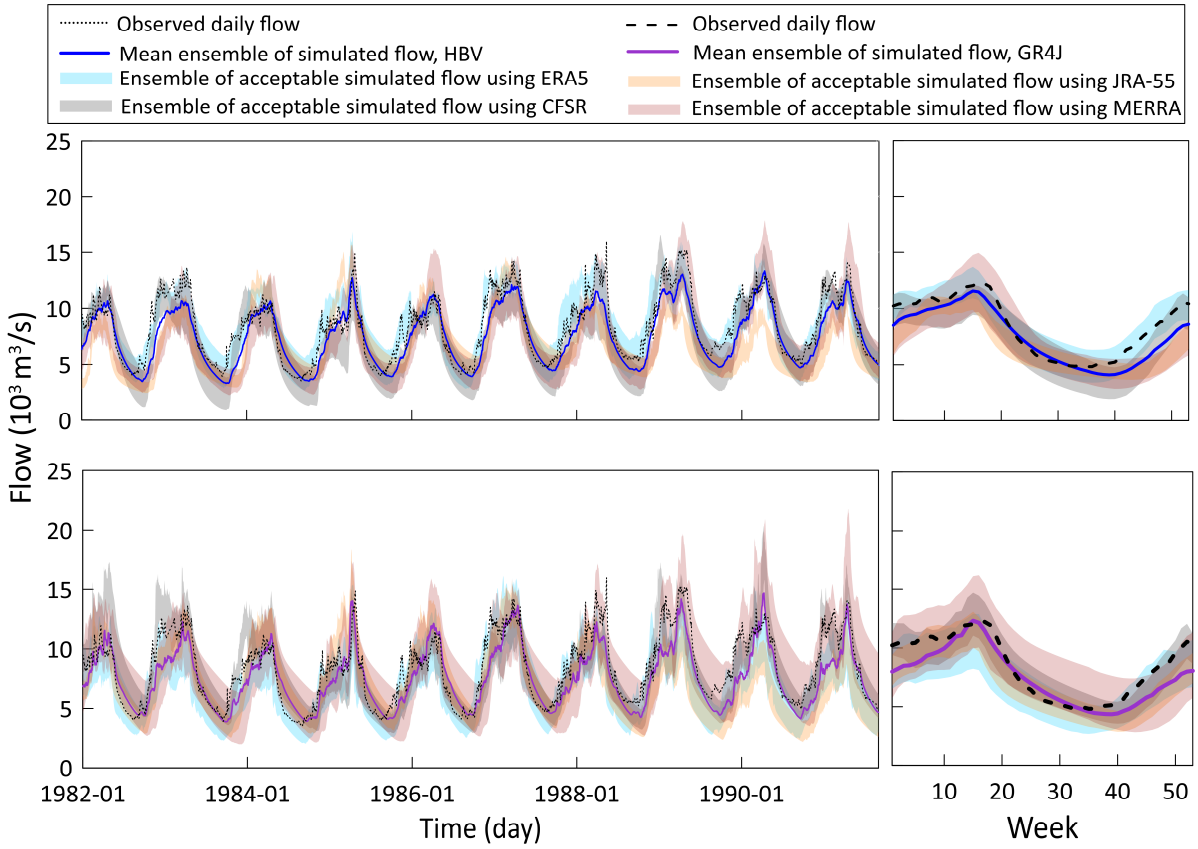

Figure 7. Comparison between the simulated (solid line and shaded areas) and observed (dashed line) expected daily (**left**) and annual (**right**) hydrographs at the outlet during the historical period using four reanalysis datasets in the calibration of hydrological models, HBV (**top**) and GR4J (**bottom**).

4.2. Calibration and Justification of HBV Model Parameters for the Kasai River Basin

While both the HBV and GR4J models are used in this research, the HBV model presents greater complexity due to its multiple routines and more extensive set of parameters, making it particularly adaptable to diverse hydrological conditions. This adaptability is especially valuable in complex catchments like the Kasai River Basin, where varying climatic and hydrological factors must be accurately represented.

The parameters of the HBV model must be carefully calibrated to reflect the specific physical and hydrological characteristics of the catchment under study. This involves adjusting parameters related to soil moisture and runoff processes to match observed data and ensure that the model outputs are physically feasible and representative of the real-world system.

Table 3 presents the calibrated parameter values for the HBV model applied to the Kasai River Basin. These parameters include the degree-day coefficient, the potential evapotranspiration (ET) coefficient, soil moisture coefficients, outlet coefficients, the percolation coefficient, and soil moisture capacity, among others.

Table 3. Calibrated parameter values for the HBV model applied to the Kasai River Basin.

Parameter	Optimized Value
Degree-day coefficient	2.28
Potential ET coefficient	0.91
Low soil moisture coefficient	0.20
Snow capacity to retain water	0.05
Topmost outlet's coefficient	0.00
Intermediate outlet's coefficient	0.01
Bottom outlet's coefficient	0.01
Percolation coefficient	0.05
Topmost outlet's trigger	48.70
Soil moisture capacity	496.90
Base of triangle delay function	1.16
Soil's water absorption coefficient	1.06
Soil's curve number	39.77
Frozen soil coefficient	N/A
Soil frost temperature threshold	N/A
Melting temperature threshold	N/A
Snow correction factor	N/A

In this section, the justifications for the physical feasibility of these calibrated parameters will be provided. Each parameter will be discussed in terms of its role in the model, its expected range based on the physical characteristics of the Kasai River Basin, and how the calibrated values align with the observed data and hydrological theory. This thorough calibration and validation process ensures that the model provides reliable simulations of hydrological processes in the basin, contributing to accurate assessments of climate change impacts and water resource management strategies.

A value of 2.28 for the degree-day coefficient is reasonable for areas with occasional snow or ice presence, likely in elevated regions. This value reflects a moderate rate of melting, which aligns with the infrequent frost or snow events in higher altitudes.

The potential evapotranspiration (ET) coefficient adjusts potential evapotranspiration to better match observed climate conditions. In the Kasai Basin, characterized by a tropical climate, high evapotranspiration rates are common. A coefficient of 0.91 indicates slightly reduced ET compared to potential rates, possibly due to soil moisture limitations or vegetation cover, making this value physically feasible.

The low soil moisture coefficient, which controls the storage capacity of the soil and affects runoff and infiltration, is set at 0.20. This low value suggests that soils in the basin have a limited capacity to retain water, leading to quick runoff. This is consistent with the characteristics of lateritic or sandy soils commonly found in tropical regions, where infiltration may be fast but retention capacity is low.

The topmost outlet's coefficient governs the fast runoff from the upper zone. A coefficient of 0.00 suggests negligible fast runoff, which could be due to the absence of steep slopes or the dominance of infiltration over surface runoff in the basin. This is plausible for a region with relatively flat terrain and dense vegetation cover.

The intermediate outlet's coefficient controls slower runoff from intermediate soil layers. A value of 0.01 indicates minimal interflow, which might be expected in a basin where most water either infiltrates deeper or runs off slowly due to gentle slopes. This value is physically feasible given the topography and soil structure in the Kasai Basin.

The bottom outlet's coefficient represents the slow release of groundwater (baseflow). This low value reflects a slow but steady contribution of groundwater to streamflow, typical of large flat basins with significant groundwater storage, such as the Kasai Basin. It ensures the model accounts for sustained baseflow during dry periods.

The percolation coefficient determines the rate at which water percolates from the upper to lower soil layers. A moderate percolation rate of 0.05 is realistic in a tropical basin

where soils have moderate permeability, balancing between rapid drainage in sandy soils and slower percolation in more clay-rich areas.

A high topmost outlet's trigger value of 48.70 indicates that significant soil moisture must accumulate before rapid runoff occurs, which is plausible in a basin with deep soils and dense vegetation that can absorb considerable water before contributing to surface runoff.

Soil moisture capacity, defining the maximum water storage capacity of the soil before excess contributes to runoff, is set at 496.90. This high value suggests that soils in the Kasai Basin have a substantial capacity to store water, which aligns with the deep well-structured soils found in many parts of the basin. It allows the model to simulate prolonged dry periods without immediate runoff.

The base of the triangle delay function represents the delay in runoff due to channel storage and routing. A value of 1.16 is moderate and suggests that water movement through the river network is relatively fast but not instantaneous. This reflects the balance between quick surface runoff and slower groundwater contributions in the basin.

The soil's water absorption coefficient controls the rate of the soil absorption of water, influencing infiltration and runoff. A value slightly above 1.0 indicates efficient water absorption by the soil, which is consistent with the dense vegetation and well-developed soil profiles in the Kasai Basin. It ensures that the model realistically simulates infiltration processes.

The soil's curve number reflects the potential for runoff based on land use, soil type, and moisture conditions. A curve number of 39.77 is low, indicating a low runoff potential, which is expected in a region with extensive forest cover, permeable soils, and moderate rainfall intensities. This ensures that the model does not overestimate surface runoff, especially during light-to-moderate rainfall events.

Ultimately, the calibration parameters for the HBV model in the Kasai River Basin are physically feasible and aligned with the basin's climatic, hydrological, and topographical characteristics. The careful calibration ensures that the model accurately simulates the hydrological processes in this tropical basin, providing reliable results for water resource management and climate impact studies.

4.3. Projected Streamflow Conditions Under Changing Climate

The outputs of 19 climate models under RCPs 4.5 and 8.5 are fed to these eight hydrological models to estimate the flow in the KARB during the future horizons. The observed and projected mean annual streamflow hydrographs at the basin's outlet under RCP 8.5 using HBV and GR4J models calibrated with four reanalyses are presented in Figure 8. The right panel in this figure shows all projected flows under these eight configurations. The results for RCP4.5 are depicted in Figure S1 in the Supplementary Materials. Overall, the models show changes in flow conditions; however, the estimated rate of change depends on the considered modeling configuration. For instance, the rate of decrease is more considerable based on the HBV than GR4J model. Indeed, the projected flow using GR4J, an ensemble of four configurations, presents no change in the near-term and mid-term future and a slight increase in the long term under a high-emission scenario. Such divergence between the results of these two models can be logical due to the noted differences in the structure and performance of these models during the historical period.

Considering the impact of reanalysis, the models calibrated using ERA5-land, CFSR, and JRA-55 show almost similar hydrographs. In contrast, MERRA-based models have considerably different hydrographs in shape and high flow magnitudes showing an increase in future high flows. The mean of projections based on all eight model configurations (right panel) reveals a slight decline in streamflow volume with no change in peak flow timing at the outlet of the KARB under RCP 8.5. Regarding RCP 4.5, one-week-early peak flow is projected for the mean annual flow during all future horizons. This reduction in flow might be due to a decrease in rainfall and an increase in the evapotranspiration caused by temperature rise. These findings are consistent with previous studies of the Congo River Basin [19,63,65,66]. For instance, Aloysius and Saiers [19] estimated prolonged periods of

low flow and runoff decline in the southern headwater areas due to rainfall decrease in comparison to their reference period of 1986–2005. They also found a runoff increase of 10.4% over the whole southwestern region under RCP 8.5 during 2046–2065.

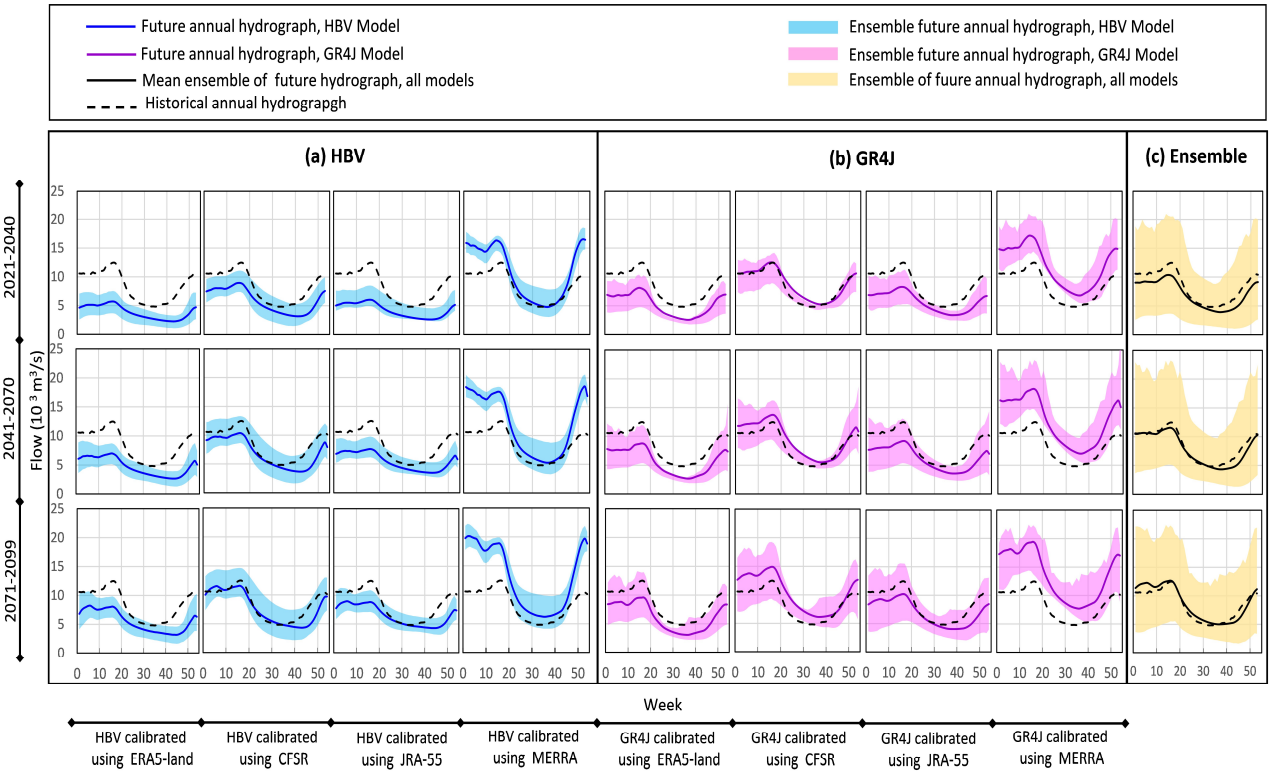

Figure 8. Observed (dashed line) versus projected ensemble (shaded area) and expected (solid line) mean annual flow hydrographs at the basin's outlet under RCP 8.5 using HBV (**a**) and GR4J (**b**) models calibrated with four reanalyses, and all configurations (**c**) using the outputs of 19 GCMs are also shown.

Such decreases in streamflow discharge can affect water resources management in the KARB. Here, the changes in 90th (Q90), 50th (Q50), and 10th (Q10) percentiles of flow are analyzed to gain a better understanding of future flow conditions based on individual and ensemble model configurations. For this purpose, the observed (recorded) and simulated annual flow duration curves (i.e., empirical cumulative probability distributions of flow in each year) are derived for both historical and future periods. The long-term mean annual quantiles for the observed flow are calculated by averaging these values over the historical period. For the future period, the annual values are calculated under each of the eight model configurations using the optimal and acceptable parameter sets, with 19 GCM outputs under RCPs 4.5 and 8.5. The relative changes between these future annual quantiles under RCPs 8.5 and 4.5 and the long-term historical values are presented in Figure 9 and Figure S2 in the Supplementary Materials, respectively. The results are shown per model configuration and as an ensemble of values per each hydrological model, followed by a boxplot containing values for all configurations.

While an overall decrease in all three flow signatures is projected considering the ensemble of all eight models, the magnitude and sign of change vary among configurations. For instance, under RCP 8.5, high flow (Q90) is expected to decrease by 40% according to HBV-ERA5 and by 22% according to GR4J-ERA5, whereas MERRA-based models estimate an increase of 50% by HBV and 57% by GR4J for Q50. Indeed, the models calibrated with MERRA datasets show completely different changes than the models calibrated with other reanalysis datasets. This model overestimates the high flows during the historical period as well. Figure 9 also shows that the GR4J-based models estimate a larger range of change

in quantiles than the HBV ones. Moreover, although both models project a decline in Q10, Q50, and Q90 in all future horizons, the percentage reduction based on HBV models is more intense. For example, Q50 is projected to decrease on average by −23% based on HBV models and −1% by GR4J models under RCP 8.5 by the late century. The results based on all model configurations (black boxplot) reveal a decline of 9%, 18%, and 13% for low, median, and high flow, respectively, under RCP 8.5. These ranges of reduction are larger under RCP 4.5, i.e., −24% for Q10, −28% for Q50, and −25% for Q90, respectively (see Figure S2 in the Supplementary Materials). This is mainly because of the higher rate of increase in mean precipitation relative to the historical period under RCP 8.5 compared to RCP 4.5 (see Figure 4a).

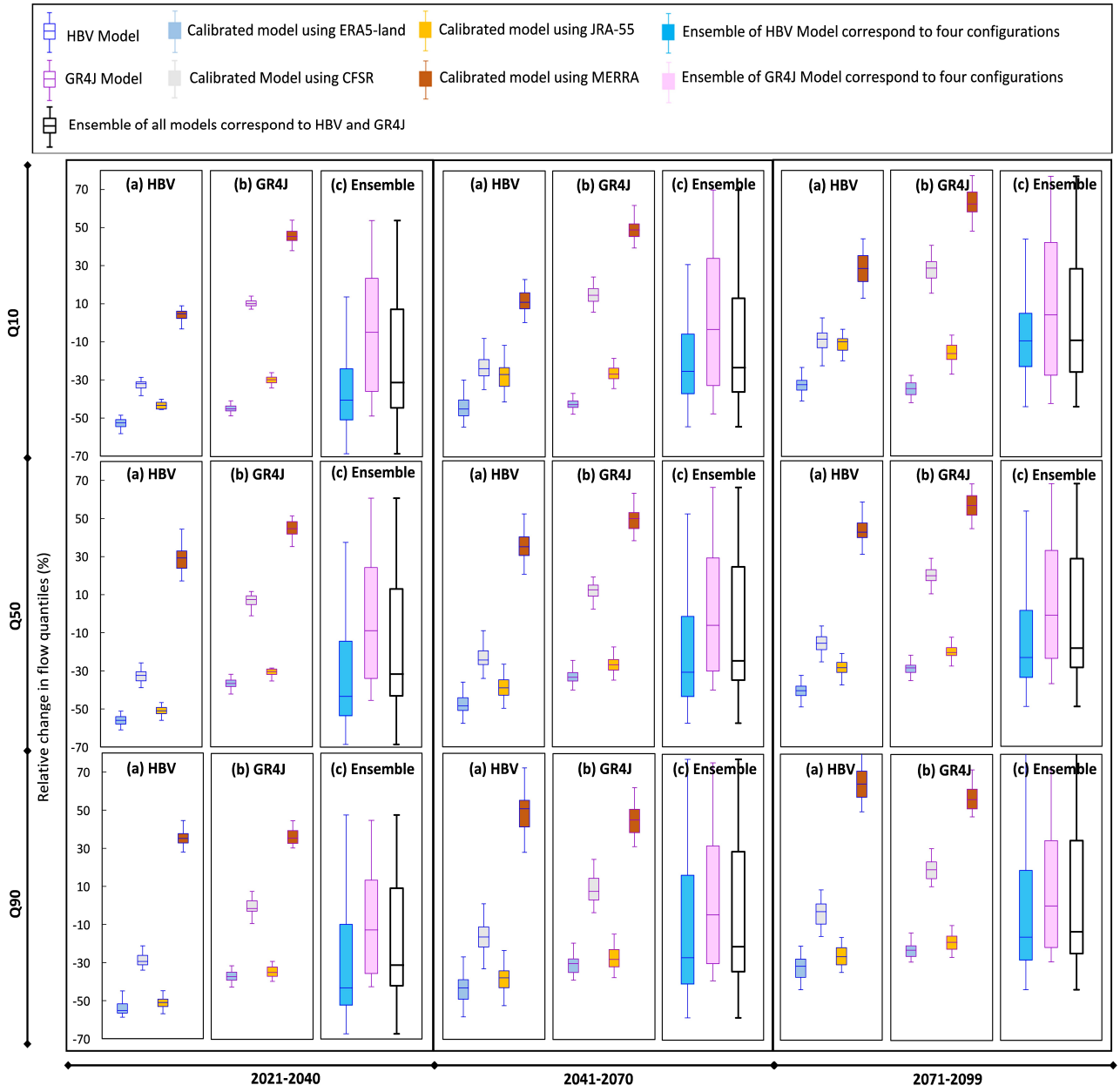

Figure 9. Relative changes between the estimated annual streamflow quantiles by individual and all model configurations fed by outputs of 19 GCMs under RCP 8.5 with respect to the long-term average historical value.

As previously noted, the values of high flows are particularly important for estimating potential hydropower production in this region. Therefore, the trend in annual Q90 over 2021–2100 is analyzed, estimated using individual and ensemble model configurations, given the acceptable and optimal parameter sets fed by 19 GCM outputs under RCPs 4.5 and 8.5 (see Figure 10). The long-term average annual Q90 of 12,030 m^3/s during the historical period is used as the benchmark (reference value). The projected trend in high flow by the ensemble of models reveals a slight decline in hydropower potential. It is evident that the estimated values and trends of Q90 in the future significantly differ among model configurations. In particular, the MERRA-based model shows a notably different trend than the others. Models calibrated with ERA5-land and JRA-55 estimate a decrease in high flow over the entire century under both scenarios. Additionally, it is noteworthy that the estimated Q90 values by GR4J using CFSR show almost no change under RCP 4.5 and a slight increase under RCP 8.5 from the middle to the end of the century. In contrast, the trendline for Q90 based on the HBV-CFSR model remains below the reference level throughout the century under both emission scenarios. Indeed, the expected values of Q90 based on all models (right panels) remain below the reference level under RCP 4.5, whereas they reach the long-term historical quantile by 2058 and slightly increase by the end of the century under RCP 8.5.

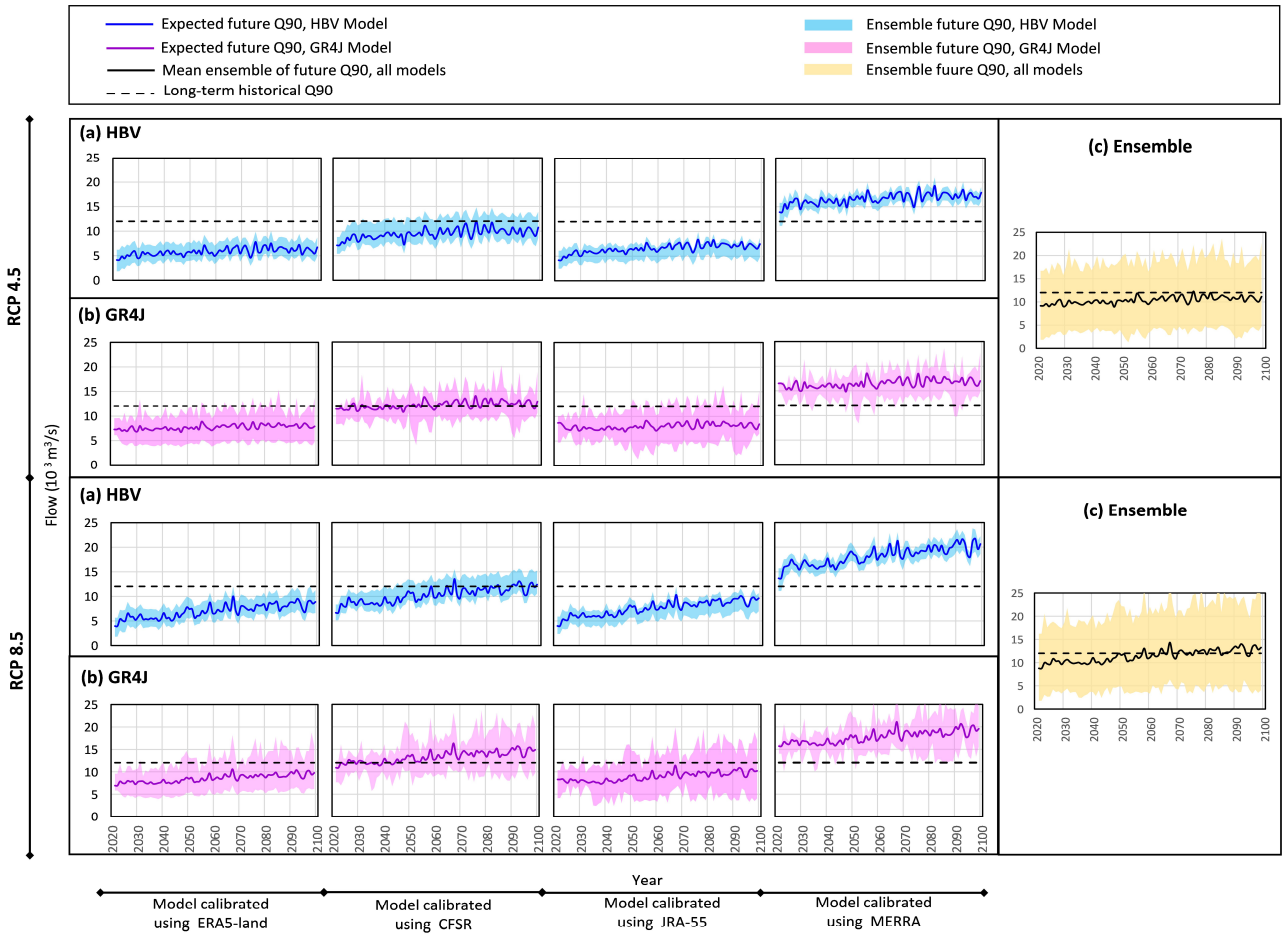

Figure 10. The ensemble (shaded area) and expected (solid line) values of annual Q90 in the future under RCPs 4.5 and 8.5 based on calibrated HBV (blue) and GR4J (pink) models using four reanalysis datasets (**left**) and all 8 model configurations (**right**). The dashed line shows the long-term annual Q90 values during the historical period.

The Mann–Kendall trend test [98], a commonly used nonparametric method in climate analysis, is employed to understand the trend and determine its significance. The *p*-values

and trend slope of expected future annual Q90 calculated for individual and ensemble configurations are presented in Table S2 in the Supplementary Materials. The significance test results reveal an increasing trend in high flow based on the ensemble of all models under both RCP 4.5 and 8.5, with significance levels of 0.05 and p-values of 4.5×10^{-10} and 1.5×10^{-18}, respectively. Notably, the trend line slope under RCP 8.5 is double that under RCP 4.5. These changes in streamflow conditions, particularly high flows, mean that decisions around constructing reservoirs and hydroelectricity generation should account for the impacts of climate change.

The gross hydropower potential for both present and future periods is estimated to provide an overall indication of relative changes in the basin [99–101]. The amount of hydropower generated from flow with the discharge of Q and head difference in H can be estimated by $P = \rho g Q H \eta$, where P is the power, ρ is the density of water, g is the gravity acceleration, and η is the overall efficiency of the turbine. The theoretical hydropower production is estimated by considering the natural drop of the KARB mainstream for the head, which is 1120 m [51]. The mean of annual high-flow Q90 obtained from the ensemble of all eight model configurations in the future is used as Q, which is equal to 10,332 and 11,436 m^3/s under RCPs 4.5 and 8.5, respectively. Accordingly, the relative change in theoretical hydroelectric generation between future and historical periods is calculated. Assuming an efficiency coefficient of 0.7 is reasonable, and the results reveal that the theoretical potential of the basin will decrease by around 14% and 5% under RCP 4.5 and RCP 8.5, respectively, in the long-term future. Such changes in hydropower potential should be considered in energy supply and development plans.

5. Summary and Conclusions

This study assesses the possible impacts of climate change on streamflow characteristics and hydropower potential using a multi-model framework over the KARB, an important watershed in the Congo River Basin, Central Africa. For this purpose, two conceptual hydrological models, HBV and GR4J, which are calibrated using four reanalysis products, are fed with 19 GCMs' bias-corrected outputs under two emission scenarios, RCPs 4.5 and 8.5. Results reveal that both hydrological models calibrated with different reanalysis datasets can simulate the observed flow in the KARB with acceptable performance. Considering both daily and annual time series, the calibrated models with ERA5-land datasets perform better, particularly in representing the peak flow timing and magnitude and low flows. Our simulations under climate change scenarios show that flow discharge is likely to decrease with no change in peak timing and seasonality. However, the estimated magnitude of change depends on the considered configuration, i.e., hydrological model and the reanalysis dataset used for calibration and the future scenario. Overall, changes in mean annual discharge ranging from −18% to +3% at the outlet of the basin in the future is estimated in comparison to the observed values. Among model configurations, MERRA-based models and GR4J-CFSR-based models show an increase in annual hydrographs, while others are similar with a declining trend. Considering flow signatures, while an overall decrease in all three quantiles (Q10, Q50, and Q90) is projected based on the ensemble of all eight modeling configurations, the magnitude and sign of change vary among configurations. Given the importance of high-flow Q90 in hydropower potential analysis, our analysis reveals that Q90 will be decreased by 25% and 13% under RCPs 4.5 and 8.5, respectively, with respect to the long-term average historical value. Consequently, the theoretical hydropower potential is expected to decline by 14% and 5% under low- and high-emission scenarios, respectively. In addition, a trend analysis reveals that annual power potential follows a significant increasing trend between 2021 and 2100 based on the ensemble of all models with a p-value of 4.5×10^{-10} and 1.5×10^{-18}. Although the mean annual flow's magnitude is below the reference line (long-term average historical value) during the future period, its trend is positive toward the end of the century. Moreover, although the projections show a decline in annual high flow, these decreased rates are not likely to create a major water supply issue for hydropower generation. Based on the

ensemble of all models, the average decrease in low-flow Q10 is projected to be 24% and 9% in the long-term future under RCP 4.5 and RCP 8.5, respectively. This decline in low flow might affect navigation, which has already been threatened by climate change in the KARB, reported by CICOS [102]. The changes in low and high flow can also have implications for aquatic life, channel maintenance, and flooding. Hence, water managers should consider these changes in policymaking and water allocations.

Our study is the first step toward a multi-model climate change impact assessment of the Congo River Basin and has some limitations. In future research with the ongoing field measurements that CICOS has planned within the KARB, one may apply hydrological models with different catchment representations (both lumped and semi-distributed models) or include more models to estimate flow. Furthermore, in this study, the GCM outputs based on the CMIP5 project are used. It is recommended to use other climate model outputs that are recently released, i.e., CMIP6, to better highlight the probable future conditions of the basin. Such analysis in the context of the applied framework can also be extended to analyze the vulnerability of other catchments in the Congo River Basin to provide an integrated impact assessment within the whole basin conditions. This integration can provide policymakers with more comprehensive knowledge for water resources, energy, agriculture, and ecosystem management. Notably, the flow projections of this study account for the changing climate and can be considered a part of an investigation of multiple stressors on water resources. It is also suggested that other key aspects such as population growth and rising water demand be considered in the development of adaptation policies.

In addition to the comprehensive findings presented in this study, it is important to acknowledge the research limitations and sources of uncertainties that may affect the results and their interpretation.

Firstly, the hydrological models used in this study, HBV and GR4J, are conceptual and have inherent simplifications in representing complex hydrological processes. The calibration of these models was based on reanalysis datasets, which, while useful, may not fully capture local hydrological dynamics or variations. The accuracy of these models is also contingent upon the quality of the input data, particularly the bias-corrected outputs from the 19 GCMs. Any inaccuracies or biases in these datasets can propagate through the modeling process, leading to uncertainties in the projections.

Secondly, the study utilized GCM outputs from the CMIP5 project, which, although robust, have been succeeded by more recent climate models under the CMIP6 project. The use of CMIP6 models could potentially offer more refined and updated projections of future climate conditions, potentially altering the impact assessments made in this study.

Additionally, the analysis does not account for other significant factors such as land use changes, population growth, and increasing water demand, which could further influence hydrological responses and water resource availability in the KARB. These factors are critical for developing comprehensive adaptation strategies and should be integrated into future research to provide a more holistic assessment.

Finally, this study provides critical insights into the potential impacts of climate change on streamflow and hydropower potential in the Kasai River Basin (KARB), a vital but understudied region. The results demonstrate significant shifts in flow regimes under various climate scenarios, with potential implications for water resource management and regional development.

Given the basin's reliance on rain-fed agriculture and its limited water storage infrastructure, adaptive strategies are necessary to mitigate risks to food security and biodiversity. These strategies include developing small-scale storage solutions, enhancing agricultural water-use efficiency, and promoting sustainable land management practices. Additionally, the basin's ecological richness necessitates integrated approaches that balance development goals with conservation priorities.

While the ensemble modeling approach provides robust projections, uncertainties remain due to variability across individual models. Future research should incorporate updated climate models, additional hydrological frameworks, and socio-economic fac-

tors to refine projections further. These efforts will support more effective planning and policymaking to address the challenges posed by climate variability in the KARB.

Supplementary Materials: The following supporting information can be downloaded at: https://www.mdpi.com/article/10.3390/hydrology11120207/s1.

Author Contributions: Conceptualization, S.L., E.H., and M.F.; methodology, S.L., S.S.Z., E.H., A.S., and M.F.; validation, S.L., S.S.Z., E.H., and M.F.; formal analysis, S.L.; investigation, S.L.; resources, S.L., S.S.Z., E.H., A.S., M.F., and E.H.; data curation, S.L.; writing—original draft preparation, S.L. and E.H.; writing—review and editing, S.L., S.S.Z., E.H., A.S., and M.F.; visualization, S.L., A.S., and E.H.; supervision, E.H. and M.F.; project administration, E.H. and M.F. All authors have read and agreed to the published version of the manuscript.

Funding: This research was partly funded by the NSERC (RGPIN-06979-2020), held by the fourth author.

Data Availability Statement: The historical hydrometric data for the outlet, Kutu-Moke station, was obtained from the International Commission for the Congo–Ubangi–Sangha Basin (CICOS). Regarding the climate data, the recorded daily precipitation, as well as minimum and maximum temperatures for the KARB, were obtained from the National Meteorological Agency (METTELSAT) of the Democratic Republic of Congo. The temperature and precipitation data for four reanalyses, namely ERA5-land, CFSR, JRA55, and MERRA, are freely available from the following sources: ERA5-land: https://www.ecmwf.int/node/18714, accessed on 10 October 2018; CFSR: http://cfs.ncep.noaa.gov/cfsr/, accessed on 17 August 2018; JRA55: https://rda.ucar.edu/datasets/ds628.0, accessed on 10 August 2018; and MERRA: https://disc.sci.gsfc.nasa.gov/mdisc, accessed on 2 August 2018. The climate model projections are freely available from the NASA Earth Exchange Global Daily Downscaled Projections at https://www.nccs.nasa.gov/services/data-collections/land-based-products/nex-gddp, accessed on 7 July 2021.

Conflicts of Interest: Author Ali Sharifinejad was employed by the company Aquanty Inc. The remaining authors declare that the research was conducted in the absence of any commercial or financial relationships that could be construed as a potential conflict of interest.

References

1. Laraque, A.; N'kaya, G.D.M.; Orange, D.; Tshimanga, R.; Tshitenge, J.M.; Mahé, G.; Nguimalet, C.R.; Trigg, M.A.; Yepez, S.; Gulemvuga, G. Recent Budget of Hydroclimatology and Hydrosedimentology of the Congo River in Central Africa. *Water* **2020**, *12*, 2613. [CrossRef]
2. Runge, J. The Congo River, Central Africa. In *Large Rivers: Geomorphology and Management*, 2nd ed.; Wiley-Blackwell: Hoboken, NJ, USA, 2022; pp. 433–456.
3. Aloysius, N.R.; Sheffield, J.; Saiers, J.E.; Li, H.; Wood, E.F. Evaluation of historical and future simulations of precipitation and temperature in central Africa from CMIP5 climate models. *J. Geophys. Res. Atmos.* **2016**, *121*, 130–152. [CrossRef]
4. UNEP. *Water Issues in the Democratic Republic of the Congo Challenges and Opportunities*; UNEP: Nairobi, Kenya, 2011.
5. IPCC. *Climate Change 2021: The Physical Science Basis. Contribution of Working Group I to the Sixth Assessment Report of the Intergovernmental Panel on Climate Change*; Masson-Delmotte, V., Zhai, P., Pirani, A., Connors, S.L., Péan, C., Berger, S., Caud, N., Chen, Y., Goldfarb, L., Gomis, M.I., et al., Eds.; Cambridge University Press: Cambridge, UK, 2021; *in press*.
6. Sidibe, M.; Dieppois, B.; Mahé, G.; Paturel, J.-E.; Amoussou, E.; Anifowose, B.; Lawler, D. Trend and variability in a new, reconstructed streamflow dataset for West and Central Africa, and climatic interactions, 1950–2005. *J. Hydrol.* **2018**, *561*, 478–493. [CrossRef]
7. Moukandi, G.; Laraque, A. A new look at hydrology in the Congo Basin, based on the study of multi-decadal chronicles. In *Congo Basin Hydrology, Climate, and Biogeochemistry*; American Geophysical: Washington, DC, USA, 2020.
8. Diem, J.E.; Ryan, S.J.; Hartter, J.; Palace, M.W. Satellite-based rainfall data reveal a recent drying trend in central equatorial Africa. *Clim. Chang.* **2014**, *126*, 263–272. [CrossRef]
9. Nicholson, S.E.; Klotter, D.; Dezfuli, A.K.; Zhou, L. New Rainfall Datasets for the Congo Basin and Surrounding Regions. *J. Hydrometeorol.* **2018**, *19*, 1379–1396. [CrossRef]
10. CSC. *Climate Change Scenarios for the Congo Basin*; Climate Service Centre Report No. 11; Haensler, A., Jacob, D., Kabat, P., Ludwig, F., Eds.; CSC: Hamburg, Germany, 2013; ISSN 2192-4058.
11. IPCC. Summary for Policymakers. In *Climate Change 2013—The Physical Science Basis: Working Group I Contribution to the Fifth Assessment Report of the Intergovernmental Panel on Climate Change, C.*; Intergovernmental Panel on Climate, Ed.; Cambridge University Press: Cambridge, UK, 2014; pp. 1–30.

12. Niang, I.; Ruppel, O.C.; Abdrabo, M.A.; Ama, E. Chapter 22 Africa. In *Climate Change 2014: Impacts, Adaptation, and Vulnerability. Part B: Regional Aspects. In Contribution of Working Group II to the Fifth Assessment Report of the Intergovernmental Panel on Climate Change*; Cambridge University Press: Cambridge, UK, 2014; pp. 1199–1265.
13. Schneider, S.H.; Semenov, S.; Patwardhan, A.; Burton, I.; Magadza, C.H.D.; Oppenheimer, M.; Pittock, A.B.; Rahman, A.; Smith, J.B.; Suarez, A.; et al. Assessing Key Vulnerabilities and the Risk from Climate Change. In *Climate Change 2007: Impacts, Adaptation and Vulnerability. Contribution of Working Group II to the Fourth Assessment Report of the Intergovernmental Panel on Climate Change*; Parry, M.L., Canziani, O.F., Palutikof, J.P., van der Linden, P.J., Hanson, C.E., Eds.; Cambridge University Press: Cambridge, UK, 2007; pp. 779–810.
14. Boko, M.; Niang, I.; Nyong, A.; Vogel, C.; Githeko, A.; Medany, M.; Osman-Elasha, B.; Tabo, R.; Yanda, P. Africa. In *Climate Change 2007: Impacts, Adaptation and Vulnerability. Contribution of Working Group II to the Fourth Assessment Report of the Intergovernmental Panel on Climate Change*; Cambridge University Press: Cambridge, UK, 2007; pp. 433–467.
15. Bhave, A.G.; Mishra, A.; Raghuwanshi, N.S. A combined bottom-up and top-down approach for assessment of climate change adaptation options. *J. Hydrol.* **2014**, *518*, 150–161. [CrossRef]
16. Sorland, S.L.; Schär, C.; Lüthi, D.; Kjellström, E. Bias patterns and climate change signals in GCM-RCM model chains. *Environ. Res. Lett.* **2018**, *13*, 074017. [CrossRef]
17. Hannah, L. Chapter 2—The Climate System and Climate Change. In *Climate Change Biology*, 2nd ed.; Hannah, L., Ed.; Academic Press: Boston, MA, USA, 2015; pp. 13–53.
18. Chen, J.; Brissette, F.P.; Leconte, R. Uncertainty of downscaling method in quantifying the impact of climate change on hydrology. *J. Hydrol.* **2011**, *401*, 190–202. [CrossRef]
19. Aloysius, N.; Saiers, J. Simulated hydrologic response to projected changes in precipitation and temperature in the Congo River basin. *Hydrol. Earth Syst. Sci.* **2017**, *21*, 4115–4130. [CrossRef]
20. Sidibe, M.; Dieppois, B.; Eden, J.; Mahé, G.; Paturel, J.-E.; Amoussou, E.; Anifowose, B.; Van De Wiel, M.; Lawler, D. Near-term impacts of climate variability and change on hydrological systems in West and Central Africa. *Clim. Dyn.* **2020**, *54*, 2041–2070. [CrossRef]
21. Zhou, L.; Tian, Y.; Myneni, R.B.; Ciais, P.; Saatchi, S.; Liu, Y.Y.; Piao, S.; Chen, H.; Vermote, E.F.; Song, C.; et al. Widespread decline of Congo rainforest greenness in the past decade. *Nature* **2014**, *509*, 86–90. [CrossRef] [PubMed]
22. Samba, G.; Nganga, D.; Mpounza, M. Rainfall and temperature variations over Congo-Brazzaville between 1950 and 1998. *Theor. Appl. Clim.* **2007**, *91*, 85–97. [CrossRef]
23. Hua, W.; Zhou, L.; Nicholson, S.E.; Chen, H.; Qin, M. Assessing reanalysis data for understanding rainfall climatology and variability over Central Equatorial Africa. *Clim. Dyn.* **2019**, *53*, 651–669. [CrossRef]
24. Washington, R.; James, R.; Pearce, H.; Pokam, W.M.; Moufouma-Okia, W. Congo Basin rainfall climatology: Can we believe the climate models? *Philos. Trans. R. Soc. B Biol. Sci.* **2013**, *368*, 20120296. [CrossRef]
25. Beck, H.E.; van Dijk, A.I.J.M.; de Roo, A.; Miralles, D.G.; McVicar, T.R.; Schellekens, J.; Bruijnzeel, L.A. Global-scale regionalization of hydrologic model parameters. *Water Resour. Res.* **2016**, *52*, 3599–3622. [CrossRef]
26. Huang, Q.; Qin, G.; Zhang, Y.; Tang, Q.; Liu, C.; Xia, J.; Chiew, F.H.S.; Post, D. Using Remote Sensing Data-Based Hydrological Model Calibrations for Predicting Runoff in Ungauged or Poorly Gauged Catchments. *Water Resour. Res.* **2020**, *56*, e2020WR028205. [CrossRef]
27. Ghebrehiwot, A.; Kozlov, D. Reanalysis dataset-based hydrologic predictions for ungauged basins. In *E3S Web of Conferences*; EDP Sciences: Les Ulis, France, 2021; Volume 264, p. 01001.
28. Bosilovich, M.G.; Chen, J.; Robertson, F.R.; Adler, R.F. Evaluation of Global Precipitation in Reanalyses. *J. Appl. Meteorol. Climatol.* **2008**, *47*, 2279–2299. [CrossRef]
29. Parker, W.S. Reanalyses and Observations: What's the Difference? *Bull. Am. Meteorol. Soc.* **2016**, *97*, 1565–1572. [CrossRef]
30. Essou, G.R.C.; Sabarly, F.; Lucas-Picher, P.; Brissette, F.; Poulin, A. Can Precipitation and Temperature from Meteorological Reanalyses Be Used for Hydrological Modeling? *J. Hydrometeorol.* **2016**, *17*, 1929–1950. [CrossRef]
31. Fuka, D.R.; Walter, M.T.; MacAlister, C.; DeGaetano, A.T.; Steenhuis, T.S.; Easton, Z.M. Using the Climate Forecast System Reanalysis as weather input data for watershed models. *Hydrol. Process.* **2013**, *28*, 5613–5623. [CrossRef]
32. Lin, R.; Zhou, T.; Qian, Y. Evaluation of Global Monsoon Precipitation Changes based on Five Reanalysis Datasets. *J. Clim.* **2014**, *27*, 1271–1289. [CrossRef]
33. Hamududu, B. *Impacts of Climate Change on Water Resources and Hydropower Systems: In Central and Southern Africa*; Norwegian University of Science and Technology: Trondheim, Norway, 2012.
34. Tshimanga, R.M.; Hughes, D.A. Basin-scale performance of a semidistributed rainfall-runoff model for hydrological predictions and water resources assessment of large rivers: The Congo River. *Water Resour. Res.* **2014**, *50*, 1174–1188. [CrossRef]
35. Munzimi, Y.A.; Hansen, M.C.; Asante, K.O. Estimating daily streamflow in the Congo Basin using satellite-derived data and a semi-distributed hydrological model. *Hydrol. Sci. J.* **2019**, *64*, 1472–1487. [CrossRef]
36. Asante, K.O.; Arlan, G.A.; Pervez, S.; Rowland, J. A linear geospatial streamflow modeling system for data sparse environments. *Int. J. River Basin Manag.* **2008**, *6*, 233–241. [CrossRef]
37. Chen, J.; Brissette, F.P.; Chaumont, D.; Braun, M. Performance and uncertainty evaluation of empirical downscaling methods in quantifying the climate change impacts on hydrology over two North American river basins. *J. Hydrol.* **2013**, *479*, 200–214. [CrossRef]

38. Nonki, R.M.; Lenouo, A.; Lennard, C.J.; Tchawoua, C. Assessing climate change impacts on water resources in the Benue River Basin, Northern Cameroon. *Environ. Earth Sci.* **2019**, *78*, 606. [CrossRef]
39. dos Santos Franciane, M.; de Oliveira Rodrigo, P.; Frederico, F.M. Lumped versus Distributed Hydrological Modeling of the Jacaré-Guaçu Basin, Brazil. *J. Environ. Eng.* **2018**, *144*, 04018056. [CrossRef]
40. Her, Y.; Chaubey, I. Impact of the numbers of observations and calibration parameters on equifinality, model performance, and output and parameter uncertainty. *Hydrol. Process.* **2015**, *29*, 4220–4237. [CrossRef]
41. Singh, S.K.; Marcy, N. Comparison of Simple and Complex Hydrological Models for Predicting Catchment Discharge Under Climate Change. *AIMS Geosci.* **2017**, *3*, 467–497. [CrossRef]
42. Tshimanga, R.; Hughes, D. Climate change and impacts on the hydrology of the Congo Basin: The case of the northern sub-basins of the Oubangui and Sangha Rivers. *Phys. Chem. Earth Parts A/B/C* **2012**, *50–52*, 72–83. [CrossRef]
43. Tshimanga, R.M. *Hydrological Uncertainty Analysis and Scenario-Based Streamflow Modelling for the Congo River Basin*; Rhodes University: Makhanda, South Africa, 2012.
44. Sharifinejad, A.; Hassanzadeh, E.; Zaerpour, M. Assessing water system vulnerabilities under changing climate conditions using different representations of a hydrological system. *Hydrol. Sci. J.* **2021**, *67*, 287–303. [CrossRef]
45. Ludwig, R.; May, I.; Turcotte, R.; Vescovi, L.; Braun, M.; Cyr, J.-F.; Fortin, L.-G.; Chaumont, D.; Biner, S.; Chartier, I.; et al. The role of hydrological model complexity and uncertainty in climate change impact assessment. *Adv. Geosci.* **2009**, *21*, 63–71. [CrossRef]
46. Yaghoubi, M.; Bavani, A.R.M. Sensitivity analysis and comparison of capability of three conceptual models HEC-HMS, HBV and IHACRES in simulating continuous rainfall-runoff in semi-arid basins. *J. Earth Space Phys.* **2014**, *40*, 153–172.
47. Seiller, G.; Anctil, F.; Perrin, C. Multimodel evaluation of twenty lumped hydrological models under contrasted climate conditions. *Hydrol. Earth Syst. Sci.* **2012**, *16*, 1171–1189. [CrossRef]
48. Viney, N.R.; Bormann, H.; Breuer, L.; Bronstert, A.; Croke, B.; Frede, H.; Gräff, T.; Hubrechts, L.; Huisman, J.; Jakeman, A.; et al. Assessing the impact of land use change on hydrology by ensemble modelling (LUCHEM) II: Ensemble combinations and predictions. *Adv. Water Resour.* **2009**, *32*, 147–158. [CrossRef]
49. Becker, M.; Papa, F.; Frappart, F.; Alsdorf, D.; Calmant, S.; da Silva, J.S.; Prigent, C.; Seyler, F. Satellite-based estimates of surface water dynamics in the Congo River Basin. *Int. J. Appl. Earth Obs. Geoinf.* **2018**, *66*, 196–209. [CrossRef]
50. GEIDCO. Global Energy Interconnection Development and Cooperation Organization. In *Research on Hydropower Development and Delivery in Congo River*; Springer: Singapore, 2020.
51. Devroey, E. *Le Kasai et son Bassin Hydrographique*; Par E. Devroey; Goemaere: Brussels, Belgium, 1939.
52. Kisangala, M.; Ntombi, M.K. Estimation des réserves régulatrices et établissement de la courbe de tarissement du bassin versant du Kasaï durant la période d'étiage à l'échelle de Lumbu. *Rev. Congo. Des Sci. Nucléaires* **2012**, *26*, 169–173.
53. Ntombi, M.K.; Kisangala, M. Impact de la lithologie et de l'hydrométrie sur la navigabilité du Kasaï en R. D. Congo. *Ann. De La Fac. Des Sci.* **2002**, 157–164. Available online: https://issr-journals.org/xplore/ijias/0017/002/IJIAS-16-140-14.pdf (accessed on 25 November 2024).
54. Laraque, A.; Mahé, G.; Orange, D.; Marieu, B. Spatiotemporal variations in hydrological regimes within Central Africa during the XXth century. *J. Hydrol.* **2001**, *245*, 104–117. [CrossRef]
55. Mbuebue, J.-M.T.; Muliwavyo, A.M.; Mwamba, V.L.; Phuati, E.P.; Bantu, A.K.M.; Keto, F.T. Time-scale characteristics of Kasai river hydrological regime variability for 1940–1999. *Int. J. Innov. Appl. Stud.* **2016**, *17*, 531–547.
56. Bultot, F. *Atlas Climatique du Bassin Congolais*; Institut national pour l'étude agronomique du Congo: Lubumbashi, Congo, 1971.
57. Munene, J.J.M.M.; Stiassny, M.L.J.; Iyaba, R.J.C.M.; Liyandja, T.L.D. Fishes of the Lower Lulua River (Kasai Basin, Central Africa): A Continental Hotspot of Ichthyofaunal Diversity under Threat. *Diversity* **2021**, *13*, 341. [CrossRef]
58. Brown, H.C.P.; Smit, B.; Somorin, O.A.; Sonwa, D.J.; Nkem, J.N. Climate Change and Forest Communities: Prospects for Building Institutional Adaptive Capacity in the Congo Basin Forests. *AMBIO* **2014**, *43*, 759–769. [CrossRef] [PubMed]
59. The International Energy Agency (IEA); the International Renewable Energy Agency (IRENA); the United Nations Statistics Division (UNSD); the World Health Organization (WHO); the World Bank. *Tracking SDG 7: The Energy Progress Report*; World Bank: Washington, DC, USA, 2021.
60. Mahe, G.; Lienou, G.; Descroix, L.; Bamba, F.; Paturel, J.E.; Laraque, A.; Meddi, M.; Habaieb, H.; Adeaga, O.; Dieulin, C.; et al. The rivers of Africa: Witness of climate change and human impact on the environment. *Hydrol. Process.* **2013**, *27*, 2105–2114. [CrossRef]
61. Nguimalet, C.-R.; Orange, D. Caractérisation de la baisse hydrologique actuelle de la rivière Oubangui à Bangui, République Centrafricaine. *La Houille Blanche* **2019**, *105*, 78–84. [CrossRef]
62. Linke, S.; Lehner, B.; Dallaire, C.O.; Ariwi, J.; Grill, G.; Anand, M.; Beames, P.; Burchard-Levine, V.; Maxwell, S.; Moidu, H.; et al. Global hydro-environmental sub-basin and river reach characteristics at high spatial resolution. *Sci. Data* **2019**, *6*, 283. [CrossRef]
63. Haensler, A.; Saeed, F.; Jacob, D. Assessing the robustness of projected precipitation changes over central Africa on the basis of a multitude of global and regional climate projections. *Clim. Change* **2013**, *121*, 349–363. [CrossRef]
64. Rowell, D.P. Sources of uncertainty in future changes in local precipitation. *Clim. Dyn.* **2012**, *39*, 1929–1950. [CrossRef]
65. Orlowsky, B.; Seneviratne, S.I. Global changes in extreme events: Regional and seasonal dimension. *Clim. Change* **2012**, *110*, 669–696. [CrossRef]
66. Arnell, N.W. Effects of IPCC SRES* emissions scenarios on river runoff: A global perspective. *Hydrol. Earth Syst. Sci.* **2003**, *7*, 619–641. [CrossRef]

67. Chen, Y.; Sharma, S.; Zhou, X.; Yang, K.; Li, X.; Niu, X.; Hu, X.; Khadka, N. Spatial performance of multiple reanalysis precipitation datasets on the southern slope of central Himalaya. *Atmos. Res.* **2021**, *250*, 105365. [CrossRef]
68. Muñoz-Sabater, J.; Dutra, E.; Agustí-Panareda, A.; Albergel, C.; Arduini, G.; Balsamo, G.; Boussetta, S.; Choulga, M.; Harrigan, S.; Hersbach, H.; et al. ERA5-Land: A state-of-the-art global reanalysis dataset for land applications. *Earth Syst. Sci. Data* **2021**, *13*, 4349–4383. [CrossRef]
69. Saha, S.; Moorthi, S.; Wu, X.; Wang, J.; Nadiga, S.; Tripp, P.; Behringer, D.; Hou, Y.-T.; Chuang, H.-Y.; Iredell, M.; et al. The NCEP Climate Forecast System Version 2. *J. Clim.* **2014**, *27*, 2185–2208. [CrossRef]
70. Kobayashi, S.; Ota, Y.; Harada, Y.; Ebita, A.; Moriya, M.; Onoda, H.; Onogi, K.; Kamahori, H.; Kobayashi, C.; Endo, H.; et al. The JRA-55 Reanalysis: General Specifications and Basic Characteristics. *J. Meteorol. Soc. Jpn. Ser. II* **2015**, *93*, 5–48. [CrossRef]
71. Rienecker, M.M.; Suarez, M.J.; Gelaro, R.; Todling, R.; Bacmeister, J.; Liu, E.; Bosilovich, M.G.; Schubert, S.D.; Takacs, L.; Kim, G.-K.; et al. MERRA: NASA's Modern-Era Retrospective Analysis for Research and Applications. *J. Clim.* **2011**, *24*, 3624–3648. [CrossRef]
72. Thrasher, B.; Maurer, E.P.; McKellar, C.; & Duffy, P.B. Technical Note: Bias correcting climate model simulated daily temperature extremes with quantile mapping. *Hydrol. Earth Syst. Sci.* **2012**, *16*, 3309–3314. [CrossRef]
73. Thrasher, B.; Xiong, J.; Wang, W.; Melton, F.; Michaelis, A.; Nemani, R. Downscaled Climate Projections Suitable for Resource Management. *Eos Trans. Am. Geophys. Union* **2013**, *94*, 321–323. [CrossRef]
74. Kwakye, S.O.; Bárdossy, A. Hydrological modelling in data-scarce catchments: Black Volta basin in West Africa. *SN Appl. Sci.* **2020**, *2*, 628. [CrossRef]
75. Lindström, G.; Johansson, B.; Persson, M.; Gardelin, M.; Bergström, S. Development and test of the distributed HBV-96 hydrological model. *J. Hydrol.* **1997**, *201*, 272–288. [CrossRef]
76. Seibert, J.; Vis, M.J.P. Teaching hydrological modeling with a user-friendly catchment-runoff-model software package. *Hydrol. Earth Syst. Sci.* **2012**, *16*, 3315–3325. [CrossRef]
77. Seibert, J.; Beven, K.J. Gauging the ungauged basin: How many discharge measurements are needed? *Hydrol. Earth Syst. Sci.* **2009**, *13*, 883–892. [CrossRef]
78. Samuel, J.; Coulibaly, P.; Metcalfe, R.A. Identification of rainfall–runoff model for improved baseflow estimation in ungauged basins. *Hydrol. Process.* **2012**, *26*, 356–366. [CrossRef]
79. Hargreaves, G.H.; Allen, R.G. History and Evaluation of Hargreaves Evapotranspiration Equation. *J. Irrig. Drain. Eng.* **2003**, *129*, 53–63. [CrossRef]
80. Perrin, C.; Michel, C.; Andréassian, V. Improvement of a Parsimonious Model for Streamflow Simulation. *J. Hydrol.* **2003**, *279*, 275–289. [CrossRef]
81. Sadegh, M.; AghaKouchak, A.; Flores, A.; Mallakpour, I.; Nikoo, M.R. A Multi-Model Nonstationary Rainfall-Runoff Modeling Framework: Analysis and Toolbox. *Water Resour. Manag.* **2019**, *33*, 3011–3024. [CrossRef]
82. Klemeš, V. Operational testing of hydrological simulation models. *Hydrol. Sci. J.* **1986**, *31*, 13–24. [CrossRef]
83. Gupta, H.V.; Kling, H.; Yilmaz, K.K.; Martinez, G.F. Decomposition of the mean squared error and NSE performance criteria: Implications for improving hydrological modelling. *J. Hydrol.* **2009**, *377*, 80–91. [CrossRef]
84. Nash, J.E.; Sutcliffe, J.V. River flow forecasting through conceptual models part I—A discussion of principles. *J. Hydrol.* **1970**, *10*, 282–290. [CrossRef]
85. Duan, Q.Y.; Gupta, V.K.; Sorooshian, S. Shuffled complex evolution approach for effective and efficient global minimization. *J. Optim. Theory Appl.* **1993**, *76*, 501–521. [CrossRef]
86. Yarpiz/ Mostapha Heris. Shuffled Complex Evolution (SCE-UA), MATLAB Central File Exchange. 2020. Available online: https://www.mathworks.com/matlabcentral/fileexchange/52862-shuffled-complex-evolution-sce-ua (accessed on 2 April 2021).
87. Price, W.L. Global Optimization by Controlled Random Search. *J. Optim. Theory Appl.* **1983**, *40*, 333–348. [CrossRef]
88. Dixon, L.C.W.; Szegö, G.P. *Towards Global Optimisation 2*; North Holland: Amsterdam, The Netherlands, 1978; Volume 2.
89. Törn, A.A. Clustering Methods in Global Optimization. *IFAC Proc. Vol.* **1986**, *19*, 247–252. [CrossRef]
90. Holland, J.H. *Adaptation in Natural and Artificial Systems: An Introductory Analysis with Applications to Biology, Control, and Artificial Intelligence*; The MIT Press: Cambridge, MA, USA, 1992.
91. Yang, J.; Reichert, P.; Abbaspour, K.C.; Yang, H. Hydrological modelling of the Chaohe Basin in China: Statistical model formulation and Bayesian inference. *J. Hydrol.* **2007**, *340*, 167–182. [CrossRef]
92. Wu, H.; Chen, B. Evaluating Uncertainty Estimates in Distributed Hydrological Modeling for the Wenjing River Watershed in China by GLUE, SUFI-2, and ParaSol Methods. *Ecol. Eng.* **2015**, *76*, 110–121. [CrossRef]
93. Mirzaei, M.; Huang, Y.F.; El-Shafie, A.; Shatirah, A. Application of the generalized likelihood uncertainty estimation (GLUE) approach for assessing uncertainty in hydrological models: A review. *Stoch. Environ. Res. Risk Assess.* **2015**, *29*, 1265–1273. [CrossRef]
94. Beven, K.; Binley, A. GLUE: 20 years on. *Hydrol. Process.* **2014**, *28*, 5897–5918. [CrossRef]
95. Beven, K.; Binley, A. The future of distributed models: Model calibration and uncertainty prediction. *Hydrol. Process.* **1992**, *6*, 279–298. [CrossRef]
96. Dakhlaoui, H.; Ruelland, D.; Tramblay, Y.; Bargaoui, Z. Evaluating the robustness of conceptual rainfall-runoff models under climate variability in northern Tunisia. *J. Hydrol.* **2017**, *550*, 201–217. [CrossRef]

97. Osuch, M.; Romanowicz, R.J.; Booij, M.J. The influence of parametric uncertainty on the relationships between HBV model parameters and climatic characteristics. *Hydrol. Sci. J.* **2015**, *60*, 1299–1316. [CrossRef]
98. Mann, H.B. Nonparametric tests against trend. *Econometrica* **1945**, *13*, 245–259. [CrossRef]
99. Ojo, O.I.; Ilunga, M.F. Application of Nonparametric Trend Technique for Estimation of Onset and Cessation of Rainfall. *Air Soil Water Res.* **2018**, *11*, 1178622118790264. [CrossRef]
100. Pandey, A.; Lalrempuia, D.; Jain, S. Assessment of hydropower potential using spatial technology and SWAT modelling in the Mat River, southern Mizoram, India. *Hydrol. Sci. J.* **2015**, *60*, 1651–1665. [CrossRef]
101. Yamba, F.D.; Walimwipi, H.; Jain, S.; Zhou, P.; Cuamba, B.; Mzezewa, C. Climate change/variability implications on hydroelectricity generation in the Zambezi River Basin. *Mitig. Adapt. Strateg. Glob. Chang.* **2011**, *16*, 617–628. [CrossRef]
102. CICOS. *International Commission of the Congo-Oubangui-Sangha Basin (CICOS), PROGRAMME DE MESURES 2016–2020*; CICOS: Gombe, Congo, 2016; Available online: www.cicos.int (accessed on 5 May 2024).